Stem Cell Reports
Article

ISSCR

OPEN ACCESS

Segregation of the stemness program from the proliferation program in intestinal stem cells

Yuan Liu,[1,4] Meimei Huang,[1,4] Xiaodan Wang,[1,4] Zinan Liu,[1] Siqi Li,[2] and Ye-Guang Chen[1,2,3,*]
[1]The State Key Laboratory of Membrane Biology, Tsinghua-Peking Center for Life Sciences, School of Life Sciences, Tsinghua University, Beijing, China
[2]Guangzhou Laboratory, Guangzhou, China
[3]School of Basic Medicine, Jiangxi Medical College, Nanchang University, Nanchang, China
[4]These authors contributed equally
*Correspondence: ygchen@tsinghua.edu.cn
https://doi.org/10.1016/j.stemcr.2023.03.007

SUMMARY

Stem cells can undergo continuous self-renewal and meanwhile retain the stemness capability to differentiate to mature functional cells. However, it is unclear whether the proliferation property can be segregated from the stemness in stem cells. The intestinal epithelium undergoes fast renewal, and the Lgr5$^+$ intestinal stem cells (ISCs) are essential to maintain homeostasis. Here, we report that methyltransferase-like 3 (*Mettl3*), a critical enzyme for N6-methyladenosine (m6A) methylation, is required for ISCs maintenance as its deletion results in fast loss of stemness markers but has no effect on cell proliferation. We further identify four m6A-modified transcriptional factors, whose ectopic expression can restore stemness gene expression in *Mettl3*$^{-/-}$ organoids, while their silencing leads to stemness loss. In addition, transcriptomic profiling analysis discerns 23 genes that can be segregated from the genes responsible for cell proliferation. Together, these data reveal that m6A modification sustains ISC stemness, which can be uncoupled from cell proliferation.

INTRODUCTION

Stem cells have the abilities to continuously self-renew themselves and to differentiate to mature functional cells under certain conditions (Cai et al., 2004; Ivanova et al., 2002; Post and Clevers, 2019; Ramalho-Santos et al., 2002). However, it is unclear whether the proliferation property can be segregated from the stemness at the molecular level. The intestinal epithelium undergoes fast renewal, and the *Lgr5*-GFP-marked intestinal stem cells (ISCs) are essential to maintain the intestinal epithelium homeostasis by refreshing themselves and simultaneously supplying progenitors that divide and migrate up to the villus as they mature into absorptive or secretory epithelial cells, while a subset of progenitor cells undergo differentiation into Paneth cells residing with stem cells at the bottom of the crypts (Barker, 2014; Clevers, 2013; Qi and Chen, 2015). The Lgr5$^+$ ISCs are a great model for investigation of tissue stem cells (Clevers, 2013). By comparing mRNAs of Lgr5$^+$ ISCs and their daughters, 384 stem cell signature genes were identified, which contain many genes associated with proliferation (Munoz et al., 2012).

m6A methylation, the most abundant modification in eukaryotic mRNAs, regulates a variety of biological processes (He and He, 2021; Zaccara et al., 2019). m6A modification is catalyzed by a multicomponent methyltransferase complex, called "writer," consisting of the methyltransferase-like 3 (METTL3), methyltransferase-like 14, Wilms' tumor 1-associating protein, vir-like m6A methyltransferase associated , and RNA binding motif protein 15 (Deng et al., 2018; Zaccara et al., 2019). This modification is dynamic and reversible and can be removed by demethylases (erasers) such as FTO and ALKBH5. m6A-modified RNAs are recognized by a variety of proteins (readers), which regulate RNA stability, splicing, nuclear export, or translation (Deng et al., 2018; Zaccara et al., 2019). Furthermore, m6A modification can regulate transcription (Shi et al., 2019; Wang et al., 2014a, 2014b).

m6A RNA methylation and its associated methyltransferase METTL3 have been shown to modulate stem cell differentiation, tissue development, and tumor progression. m6A RNA methylation is required for differentiation of embryonic stem cells and neural stem cells (Batista et al., 2014; Cao et al., 2020; Geula et al., 2015; Yoon et al., 2017), while m6A modification has also been shown to be crucial for self-renewal of hematopoietic stem cells (Vu et al., 2017; Weng et al., 2018; Zhang et al., 2017), glioblastoma stem cells (Cui et al., 2017), and embryonic neural stem cells (Wang et al., 2018). METTL3 has been shown to promote the colorectal cancer progression (Li et al., 2019; Shen et al., 2020; Zhu et al., 2020), and YTH N6-methyladenosine RNA binding protein F1 (YTHDF1) is critical for the ISC maintenance during regeneration and tumorigenesis (Han et al., 2020). However, the role of METTL3 in the maintenance of ISCs during homeostasis remains unknown.

In this study, we show that METTL3 is required for ISC maintenance during intestinal epithelium homeostasis, and its deletion results in impaired stemness but not proliferation. Transcriptomic profiling analysis discerns 23 stemness genes that are specifically expressed in ISCs and can be segregated from the genes responsible for cell proliferation. We have further identified four transcriptional factors whose mRNAs undergo METTL3-mediated

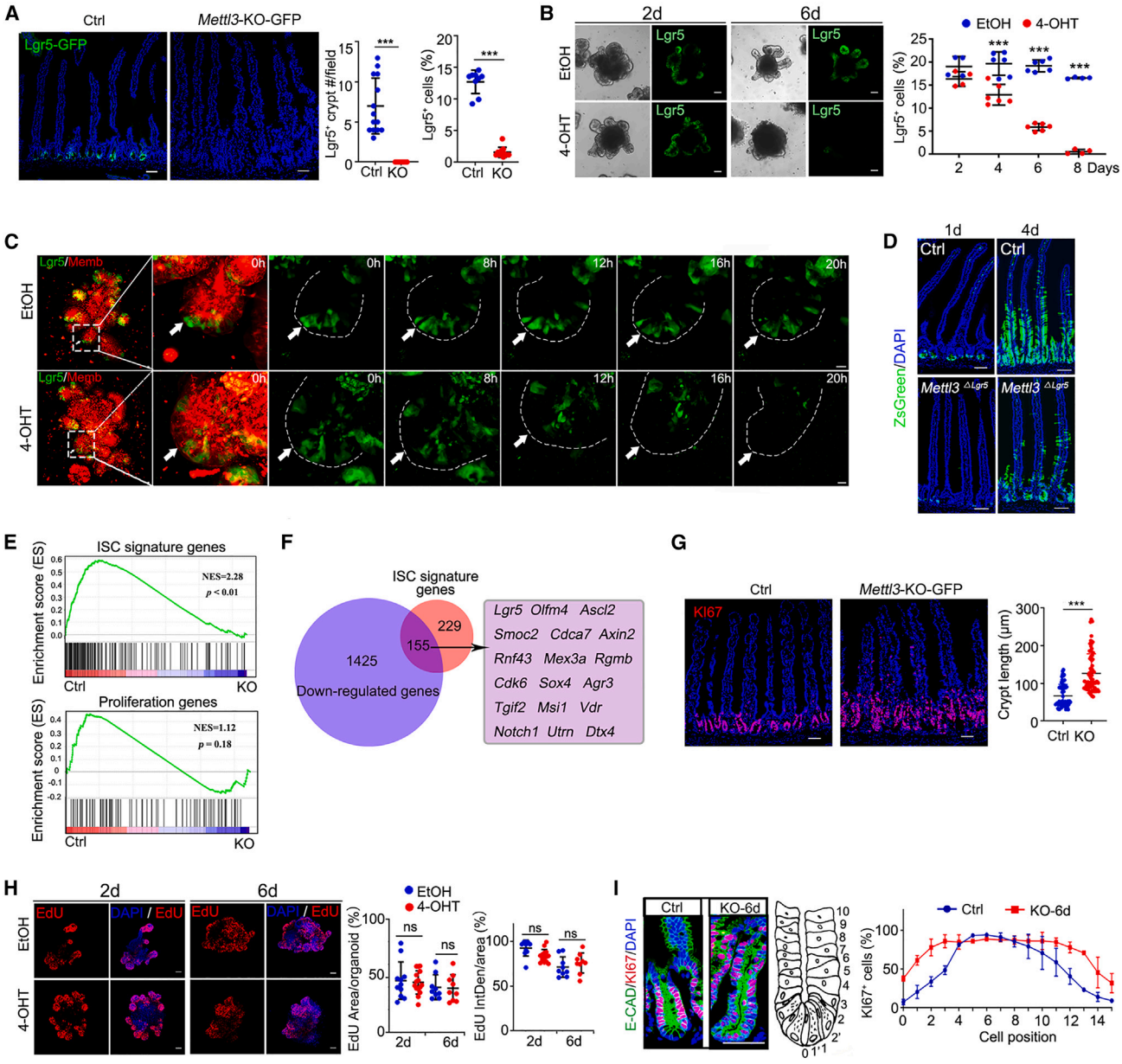

Figure 1. *Mettl3* deletion disrupts intestinal stem cells but not cell proliferation

(A and B) Representative images and quantification of Lgr5-GFP^{+} cells in the jejunum of control and *Mettl3*-KO-GFP mice at 6 dpt (A) or organoids at 2 or 6 dpt (B). N = 3 mice per group, n = 15 fields per group (A). Data from three independent experiments were combined and shown (B).

(C) Time-lapse imaging of Lgr5-GFP^{+} organoid after EtOH or 4-OHT treatment. The organoid boundary was marked with the dotted line; see also Movie S1.

(D) Lineage tracing of Lgr5^{+} cells in the jejunum of control *(Lgr5-CreERT2;Rosa26$^{loxp\text{-}stop\text{-}loxp\text{-}ZsGreen}$)* and *Mettl3$^{\Delta Lgr5}$* (*Mettl3$^{fl/fl}$;Lgr5-CreERT2;Rosa26$^{loxp\text{-}stop\text{-}loxp\text{-}ZsGreen}$*) mice at 1 or 4 dpt.

(E) GSEA of RNA-seq data from control and *Mettl3*-KO-GFP mice at 6 dpt.

(F) Venn diagram displaying the overlap between the ISC signature and the downregulated genes in *Mettl3*-KO-GFP Lgr5^{+} cells at 6 dpt.

(G) Representative images of KI67^{+} cells and quantification of crypt length in the control and *Mettl3*-KO-GFP jejunum at 6 dpt. N = 3 mice per group, n > 80 crypts per group.

(H) Representative images and quantification of EdU^{+} cells in organoids at 2 or 6 dpt. IntDen: integrated density. N > 9 organoids per group from three independent experiments.

(legend continued on next page)

m6A modification, and their ectopic expression can restore stemness gene expression in Lgr5$^+$ ISCs.

RESULTS

Mettl3 is required for small intestine maintenance

To examine whether RNA m6A modification plays a role in the homeostatic maintenance of the intestinal epithelium, we first examined the expression pattern of the m6A transferase *Mettl3*. Immunohistochemical staining and q-PCR revealed that *Mettl3* was enriched at the base of crypts (Figures S1A and S1B). To explore the role of *Mettl3* in the intestinal epithelium, we generated inducible *Mettl3* conditional knockout (KO) *Villin-CreERT2;Mettl3$^{fl/fl}$* (*Mettl3*-KO) mice (Figures S1C and S1D). Tamoxifen-induced deletion of *Mettl3* resulted in a rapid-onset body weight loss and death in ~7–11 days (Figures S1E and S1F). Morphologically, the small intestine of *Mettl3*-KO mice displayed an enlarged crypts zone at 6 days post-tamoxifen treatment (dpt), and the crypt structure disappeared with progressive shortened villus at 8 dpt (Figure S1G). Consistently, the organoids derived from *Mettl3*-KO mouse crypts, upon 4-hydroxytamoxifen (4-OHT)-induced *Mettl3* deletion, displayed an impaired growth ability, increased dying cells, and reduced budding (Figures S1H–S1J). These data indicate a critical role of *Mettl3* in the maintenance of the intestinal epithelium homeostasis.

Mettl3 deletion leads to loss of intestinal stem cells but has no effect on cell proliferation

To dissect the function of *Mettl3*, we crossed *Lgr5-EGFP-IRES-CreERT2* mice with *Villin-CreERT2;Mettl3$^{fl/fl}$* mice to obtain *Villin-CreERT2;Lgr5-EGFP-IRES-CreERT2;Mettl3$^{fl/fl}$* (*Mettl3*-KO-GFP) mice, which could label stem cells and analyze the transcriptome of ISCs. To rule out the possible non-specific effect of tamoxifen on mice or organoids, we treated *Villin-CreERT2;Lgr5-EGFP-IRES-CreERT2* mice with tamoxifen or *Villin-CreERT2;Lgr5-EGFP-IRES-CreERT2*-derived organoids with 4-OHT compared with controls, and we found that tamoxifen and 4-OHT did not cause any phenotypic changes (Figure S2). *Mettl3* KO significantly decreased Lgr5-GFP ISCs in the small intestine at 4 dpt, which was almost undetectable at 6 dpt as revealed by fluorescence-activated cell sorting (FACS) analysis and immunostaining (Figures 1A and S3A). Similar data were observed in the colon and the organoids derived from the *Mettl3*-KO-GFP mice (Figures 1B, S3B, and S3C). *Mettl3* deletion-induced disappearance of Lgr5$^+$ stem cells could be captured in the organoid by time-lapsed confocal microscopy (Figures 1C and S3D and Movie S1). The ISC marker OLFM4 was no longer detected at the crypt base of KO mice at 8 dpt (Figure S3E). In line with it, lineage tracing revealed that *Mettl3* deletion resulted in reduction of Lgr5$^+$ cells (Figures 1D and S3F). These data indicate that *Mettl3* plays a critical role in stem cell maintenance.

RNA-seq analysis revealed that *Mettl3* deletion resulted in reduced expression of most of the stem cell signature genes (Munoz et al., 2012) in ISCs from *Mettl3*-KO-GFP mice, including *Lgr5*, *Olfm4*, *Ascl2*, and *Smoc2* (Figures 1E, 1F, and S3G), which were confirmed by q-PCR (Figure S3H). Interestingly, we found that *Mettl3* deletion did not disrupt cell proliferation (Figures 1G–1I, S3I, and S3J). In fact, the longer crypts with more proliferative cells were detected in *Mettl3*-KO-GFP mice, and consistently, more crypt epithelial cells and Lgr5$^+$ ISCs were detected in the G2/M and S phase (Figure S3K). We also detected cell death at the base of crypt in KO-4d and KO-6d mice (Figure S3L). Cell differentiation was slightly affected by *Mettl3* KO as goblet cells, enteroendocrine cells, and Paneth cells were transiently increased at 6 dpt, but all intestinal cell types reduced at 8 dpt (Figures S4A and S4B), which was consistent with higher expression of the differentiation genes in the KO-4d Lgr5$^+$ cells (Figures S4C and S4D). Taken together, these results indicate that *Mettl3* deletion deteriorates the ISC stemness but not cell proliferation.

To uncover the role of *Mettl3* in ISCs, we generated a stem cell-specific *Mettl3* KO mouse, *Lgr5-EGFP-IRES-CreERT2;-Mettl3$^{fl/fl}$* (*Mettl3-Lgr5*-KO). As expected, the expression of stem cell signature genes, including *Lgr5* and *Olfm4*, was decreased in *Mettl3-Lgr5*-KO ISCs (Figure 2A). Similar to the results in *Mettl3*-KO-GFP mice, a significant decrease of Lgr5$^+$ ISCs was detected in *Mettl3-Lgr5*-KO mice at 26 dpt (Figures 2B and 2C). KI67$^+$ cells were observed in *Mettl3-Lgr5*-KO mice at 15 dpt, and differentiated cells remained similar (Figure 2D). To test the self-renewal ability of Lgr5$^+$ ISCs *in vitro* (Sato et al., 2009), we seeded with an equal number of single Lgr5$^+$ ISCs and induced *Mettl3* deletion by 4-OHT at the seeding time. Fewer organoids with *Mettl3* KO indicated that the colony forming potential was compromised in *Mettl3*-KO ISCs (Figure 2E).

Mettl3 deletion downregulates the stem cell signature genes

To monitor the cell lineage alteration upon *Mettl3* deletion, we performed single-cell RNA-seq of small intestinal

(I) Representative images and quantification showing KI67$^+$ cell position in control and *Mettl3*-KO-GFP crypts at 6 dpt. N = 3 mice per group, n = 15 fields per group. Organoids cultured from crypts of *Villin-CreERT2;Lgr5-EGFP-IRES-CreERT2;Mettl3$^{fl/fl}$* mice were treated with EtOH or 4-OHT (B, C, H). Data represent mean ± SD. ***p < 0.001, unpaired two-tailed t test (A, G), two-way ANOVA (B, H, I). Scale bars: 10 μm (C), 50 μm (A, B, D, G, H, and I). Nuclei were counter-stained with DAPI. See also Figures S1–S4 and Table S1.

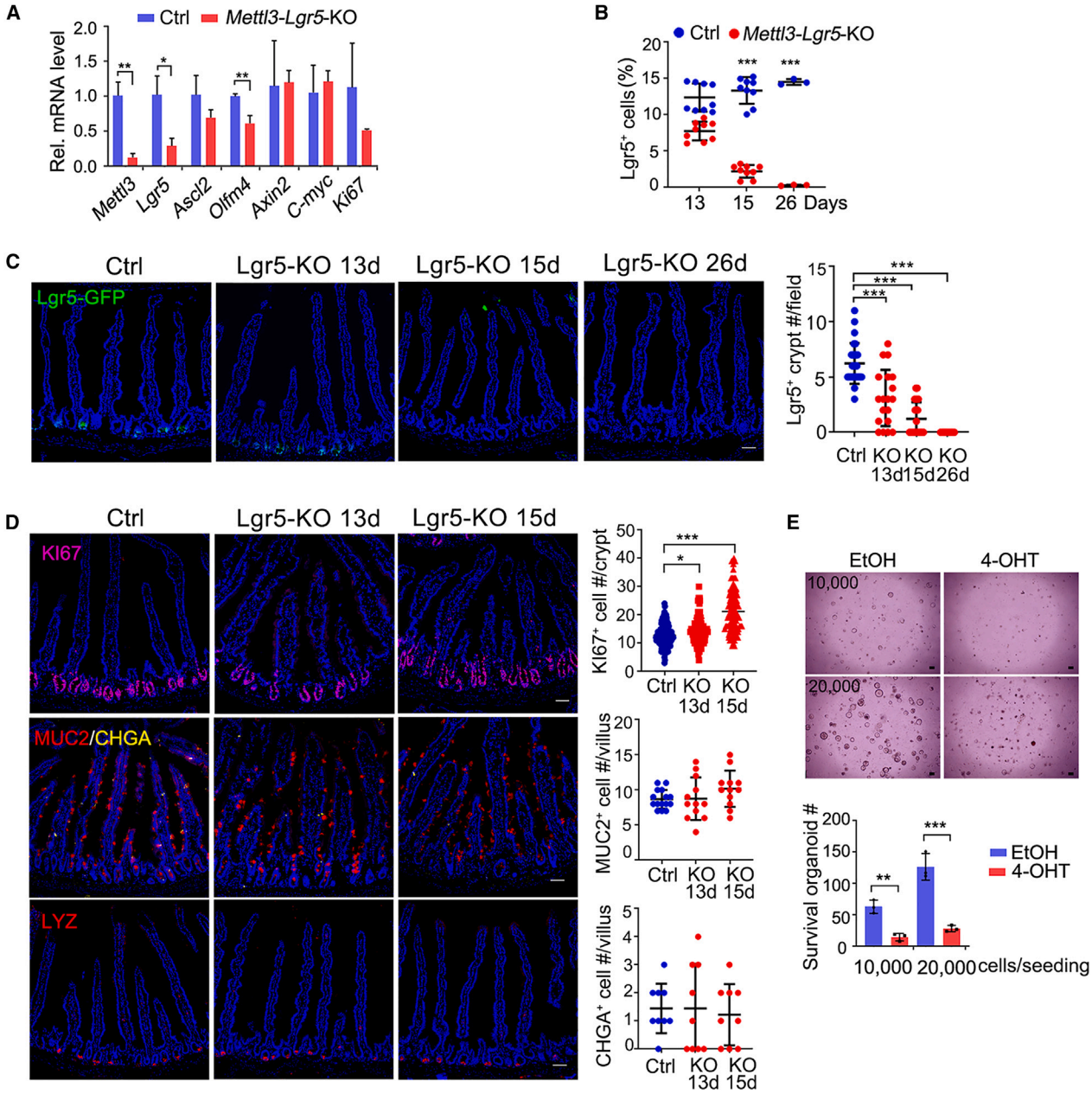

Figure 2. *Mettl3* is essential for the stemness maintenance in Lgr5$^+$ intestinal stem cells

(A) q-PCR analysis of *Mettl3*, the ISCs marker genes (*Lgr5*, *Ascl2*, *Olfm4*, *Axin2*), and the proliferation marker gene *Ki67* in FACS-sorted Lgr5-GFP$^+$ cells from control and *Mettl3-Lgr5*-KO mice at 13 dpt. N = 3 mice per group.

(B) Quantitation of Lgr5-GFP$^+$ cells in control and *Mettl3-Lgr5*-KO mice at the indicated time. N = 3 mice per group.

(C) Representative immunofluorescence images and quantification of Lgr5-GFP in the jejunum of control and *Mettl3-Lgr5*-KO mice at the indicated time. N = 3 mice per group, n = 9–15 fields per group.

(D) Representative immunofluorescence images and quantification of KI67 staining, MUC2 staining, CHGA staining, and LYZ staining in the jejunum of control and *Mettl3-Lgr5*-KO mice at the indicated time. N = 3 mice per group, n = 9–15 fields per group.

(E) Representative images (top) and quantification (bottom) of intestinal organoids cultured from sorted Lgr5-GFP$^+$ cells derived from *Villin-CreERT2;Lgr5-EGFP-IRES-CreERT2;Mettl3$^{fl/fl}$* mice after being treated with EtOH or 4-OHT for 5 days. The numbers of seeded cells were 10,000 and 20,000. Data from three independent experiments were combined and are shown. All the data represent mean ± SD. ***p < 0.001, **p < 0.01, *p < 0.05, two-way ANOVA (A, B, E), one-way ANOVA (C, D). Scale bars: 50 μm (C, D), 100 μm (E). Nuclei were counter-stained with DAPI. See also Table S2.

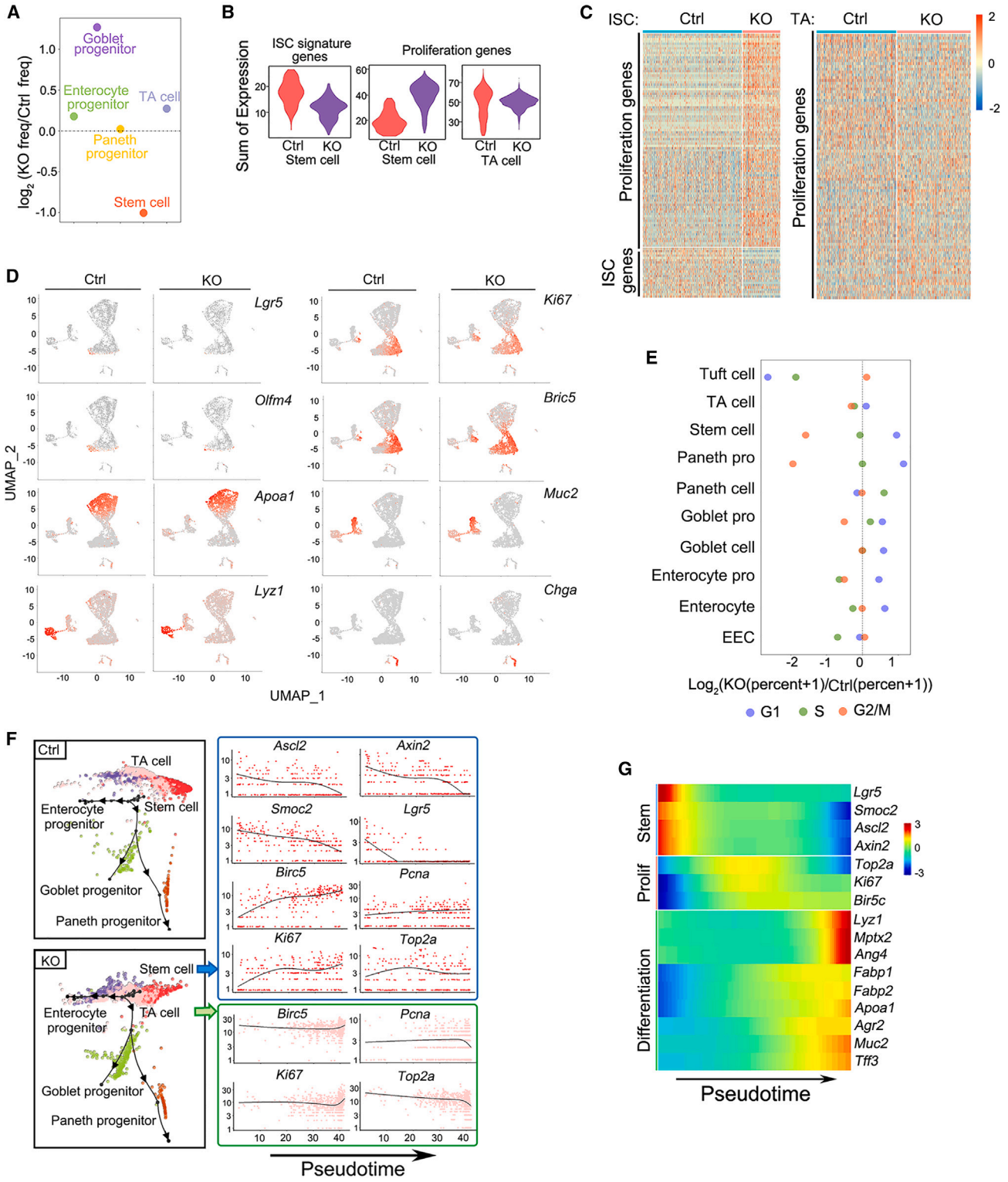

Figure 3. *Mettl3* deletion results in downregulation of the stem cell signature genes

(A) Dot plot depicting the relative frequency of stem cells, TA cells, and progenitor cells in control and *Mettl3*-KO-GFP mice at 4 dpt, revealed by scRNA-seq.

(legend continued on next page)

epithelial cells from control and *Mettl3*-KO-GFP mice at 4 dpt. Quality control selected 7,865 cells (4,467 control cells and 3,398 KO cells) for further analysis. By unsupervised clustering combined with cell-known marker genes, we identified distinct clusters, including stem cells (*Lgr5*, *Olfm4*, and *Ascl2*), transient amplifying (TA) cells (*Ki67*, *Tubb5*, and *Birc5*), goblet cells (*Tff3*, *Agr2*, and *Muc2*), Paneth cells (*Lyz1*, *Ang4*, and *Mptx2*), enteroendocrine cells (*Chga*, *Chgb*, and *Sct*), enterocytes (*Apoa1*, *Fabp1*, and *Fabp2*), tuft cells (*Dclk1*, *Gfi1b*, and *Rgsl3*), and progenitors (Figures S5A–S5C). Comparison of the abundance of each cell type unveiled a decrease of ISCs and an increase of goblet progenitor cells in the KO-4d epithelium (Figures 3A and S5D), consistent with a transient increase of goblet cells in KO-6d (Figures S4A and S4B). In line with it, *Mettl3* deletion reduced the expression of stem cell signature genes but elevated proliferation gene levels in ISCs (Figures 3B–3D) and resulted in more stem cells in the G2/M phase (Figure 3E). To deduce the dynamic change of gene expression, we used the PAGA Tree (Dyno) and DDRTree (Monocle 2) to derive pseudotime trajectories, designating high expression of ISC markers as the start point and mature lineage as the end (Figures 3F and S5E). Stem cell signature genes, like *Ascl2*, *Axin2*, *Smoc2*, and *Lgr5*, declined along the pseudotime, while the proliferation genes *Ki67*, *Pcna*, *Birc5*, and *Top2a* increased gradually in KO stem cells (Figures 3F and S5F). Differentiation genes were enriched in *Mettl3*-KO cells (Figure 3G). These results together suggest that *Mettl3* deficiency disrupts the stemness program in ISCs.

Stem cells have been defined to have the capacity to renew themselves and the ability to generate differentiated daughter cells (Ivanova et al., 2002; Post and Clevers, 2019; Ramalho-Santos et al., 2002). Great efforts have been taken to search for the genes responsible for these stem cell properties, but these kinds of genes are still elusive (Post and Clevers, 2019; Vogel, 2003). The above data showed that *Mettl3* KO reduced the expression of the stem cell markers, but not proliferation genes, suggesting that the program to maintain stemness could be uncoupled from proliferation. By comparing their expression in $Lgr5^+$ ISCs and their daughter cells, 384 genes enriched in $Lgr5^+$ ISCs were together defined as $Lgr5^+$ ISC signature genes (Munoz et al., 2012), but some of these genes are associated with proliferation. To separate the stemness genes from the proliferation genes, we characterized the differentially expressed genes in stem cells and TA cells from control or *Mettl3*-KO-GFP mice at single-cell level and found that these genes could be divided into three groups: the ISC signature genes (Munoz et al., 2012) and genes involved in proliferation (Tirosh et al., 2016) and regeneration (Liu and Chen, 2020; Wang et al., 2019) (Figure 4A). The ISC signature genes, such as *Lgr5*, *Olfm4*, *Cdca7*, and *Gkn3*, were downregulated in *Mettl3*-KO stem cells, while the proliferation genes did not change much in stem cells. Some of the ISC signature genes were found in TA cells as they may be related to cell proliferation, like *Cenpf* (Munoz et al., 2012). The regeneration genes were elevated in KO cells, probably due to the cell state associated with death-induced stress (Li et al., 2010). To better define the genes associated with stemness and exclude the ones related to proliferation, we analyzed the stem cell signature genes in our bulk RNA-seq and single-cell RNA sequencing (scRNA-seq) as well as the data from Gu et al. (Gu et al., 2021), and we found that 23 genes, including the previously described ISC-specific genes *Lgr5*, *Ascl2*, and *Olfm4*, were highly enriched in $Lgr5^{high}$ cells, and most of them decreased in $Lgr5^{low}$ cells and *Mettl3*-KO stem cells (Figures 4B–4E), suggesting that these 23 genes could be defined as the stemness genes to mark ISCs.

To explore the signaling events and/or factors that regulate the ISC stemness, we compared the differentially expressed genes in $Lgr5^+$ ISCs from control and *Mettl3*-KO-GFP mice at different time points post-tamoxifen injection (Figure S5G). *Mettl3* KO led to a decreased expression of the genes involved in Wnt and Notch signaling

(B) Violin plots showing the metagene expression levels per single cell of the stem cell signature genes and proliferation genes in stem cells and TA cells of control and *Mettl3*-KO-GFP mice at 4 dpt revealed by scRNA-seq.

(C) Expression heatmap of the stem cell signature genes and proliferation genes in stem cells (left) and TA cells (right) in control and *Mettl3*-KO-GFP mice.

(D) Expression of the stem cell marker genes (*Lgr5*, *Olfm4*), the proliferation marker genes (*Ki67*, *Birc5*), and the differentiation cell marker genes (*Apoa1*, *Lyz1*, *Muc2*, *Chga*) in intestinal epithelium from control and *Mettl3*-KO-GFP mice were plotted by UMAP. Color from gray to red indicates relative expression levels from low to high.

(E) Dot plot depicts the relative percent of the cells in the G1, G2/M, and S phase in control and *Mettl3*-KO-GFP mice.

(F) Pseudotime analysis of stem cells, TA cells, and progenitor cells in control and *Mettl3*-KO-GFP mice at 4 dpt based on scRNA-seq (left). The expression of stem cell markers (*Ascl2*, *Axin2*, *Smoc2*, and *Lgr5*) and proliferation markers (*Birc5*, *Top2a*, *Ki67*, and *Pcna*) in stem cells and TA cells of *Mettl3*-KO-GFP mice was plotted along the pseudotime axis (right).

(G) Heatmap showing the transcription trends of marker genes of stem cells, TA cells, and differentiated cells along the pseudotime. Color scale represents *Z* score normalized expression levels. The pseudotime line contains all control and *Mettl3*-KO-GFP cells with the control cell cluster as the starting point. See also Figure S5.

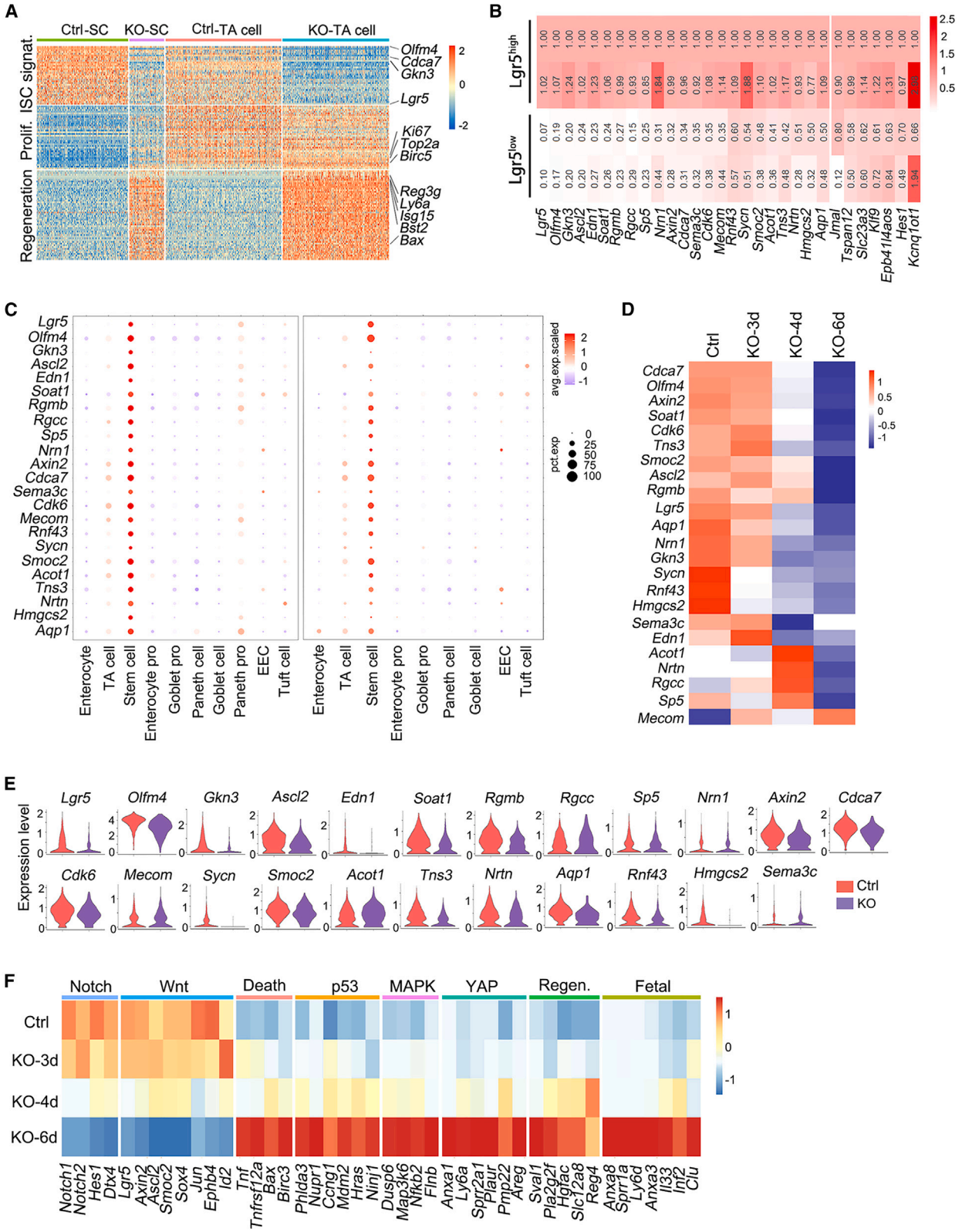

(legend on next page)

(Figures 4F and S5H), consistent with the critical role of these two signaling pathways in ISC maintenance (Clevers, 2013; Qi and Chen, 2015; Zhu et al., 2021). Most of the stemness genes were further downregulated in *Mettl3*-KO ISCs at later time points (Figure 4D), while the genes related to cell death, P53, MAPK, YAP, regeneration, and fetal signature genes were upregulated (Figures 4F and S5H). These changes indicate that *Mettl3* deletion leads to loss of stemness but not proliferation and enhanced regeneration and cell death.

ASCL2, KLF9, FOSB, and PURB collaborate to regulate stemness gene expression

To identify potential targets regulated by METTL3-mediated m6A modification, we performed methylated RNA immunoprecipitation (MeRIP)-seq in Lgr5^{high} ISCs and found that 2,074 transcripts showed a reduced m6A modification in Lgr5^{high} ISCs from *Mettl3*-KO-GFP mice. Most of the targets contained the common m6A motif "RRACH (GGACU)" in the protein-coding region and 3′ UTR, especially enriched near the stop codon (Figures S6A–S6C). In the 2,074 transcripts, 831 were downregulated (clusters 3 and 5) in *Mettl3*-KO ISCs, and among the 293 with more than 2-fold decrease in expression, 66 were transcriptional factors (TFs) (Figures 5A, 5B, and S6D). Interestingly, the genes in cluster 5 reduced in *Mettl3*-KO Lgr5^{+} ISCs at 3 dpt were also involved in transcription regulation (Figure 5C). To identify the TFs responsible for the impaired stemness, we focused on the TFs that are m6A modified and downregulated at early time points upon *Mettl3* deletion. By the combinatory analysis of bulk RNA-seq and MeRIP-seq data and q-PCR confirmation, we sifted out 10 TFs (Figures 5D–5F).

Among them, *Ascl2*, *Klf9*, *Fosb*, and *Purb* (*AKFP*) are the top TFs that might regulate the expression of the 384 ISC signature genes (Munoz et al., 2012) and the 23 stemness genes. Consistently, prediction of the binding sites of AKFP in the genome with JASPAR, TRANFAC, and HOMER revealed more than 4,000 possible target genes that are mainly enriched for stem cell signature genes and Wnt and Notch signaling (Figures S6E–S6G). To further address whether METTL3-mediated m6A binding sites of 3′ UTR are required for RNA stability modulation, we analyzed the m6A modification sequence through MeRIP-seq (Figure 5G), performed the *AKFP* 3′ UTR-reporter luciferase assay and found that *Mettl3* KO decreased the activity of the luciferase construct containing 3′ UTR (Figure 5H). Mutation of all these sites (A to T) rendered resistance to the effect of *Mettl3* KO. Therefore, METTL3 regulates the stability of these TF transcripts dependent on its m6A methyltransferase activity.

To determine whether these TFs are the key factors controlling ISC stemness, we performed rescue experiments in organoids derived from the crypts of *Mettl3*-KO-GFP mice by ectopically expressing *AKFP* and knockout assay in the organoids derived from the crypts of *Rosa26*$^{loxp\text{-}stop\text{-}loxp\text{-}Cas9\text{-}EGFP}$ mice. As shown in Figures 6A–6D, expression of *AKF* (*Ascl2*, *Klf9*, and *Fosb*) and *AKFP* was able to restore Lgr5^{+} ISCs and budding number of *Mettl3*-KO-GFP organoids. Conversely, *AKFP*-KO organoids resulted in reduced cell survival rate, downregulated ISC signature genes, and subsequent cell death (Figures 6E–6G). Transcriptome profile analysis revealed that only *AKFP* could better rescue some of the 23 stemness genes (Figure 6H). In contrast, ectopic expression of individual factors only partially restored morphology, survival rate, budding, and Lgr5^{+} ISC number in *Mettl3*-KO-GFP organoids (Figures S6H–S6J). Furthermore, *AKFP*-KO organoids exhibited decreased 23 stemness genes expression (Figure 6I). These results suggest that *AKFP*, but not any single one, can restore Lgr5^{+} ISCs to a certain extent.

We further predicted the possible downstream target genes of these TFs and found that the stem cell signature genes were enriched (Figures 6J and S6K). In agreement with it, based on the binding motif of FOSB (Figure S6L), FOSB bound to around 36% of predicated stem cell signature genes as showed by ChIP-seq (Figure S6M), for instance, the stemness genes *Lgr5*, *Edn1*, *Ascl2*, and *Rnf43* but not the proliferation genes *Ki67* and *Birc5* (Figures 6K and S6N). These binding sites were correlated with the chromatin accessibility as shown by assay for transposase-accessible chromatin with sequencing (ATAC-seq) analysis. These data together indicate that METTL3-mediated m6A

Figure 4. Identification of the stemness genes via bulk RNA-seq and scRNA-seq analysis

(A) Heatmap of differentially expressed genes in stem cells and TA cells of control and *Mettl3*-KO-GFP mice at 4 dpt based on scRNA-seq.

(B) RNA-seq analysis of the relative expression of genes, which were enriched in Lgr5^{high} cells in control mice.

(C) scRNA-seq analysis showing the gene expression level (color scale) and expressing cells (point diameter) in each cell cluster of the intestinal epithelium. All of these genes were sifted out of the gene list (B) showing specific expression in stem cells in our scRNA-seq data (left) and published ileum scRNA-seq data (right).

(D) Expression heatmap of the filtered 23 stemness genes in Lgr5^{+} ISCs of control and *Mettl3*-KO-GFP mice at 3, 4, and 6 dpt, based on bulk RNA-seq.

(E) Violin plots showing the expression of the 23 stemness genes in stem cells of control and *Mettl3*-KO-GFP mice.

(F) Expression heatmap of different pathway genes in Lgr5^{+} ISCs of control and *Mettl3*-KO-GFP mice at 3, 4, and 6 dpt, based on bulk RNA-seq. See also Figure S5.

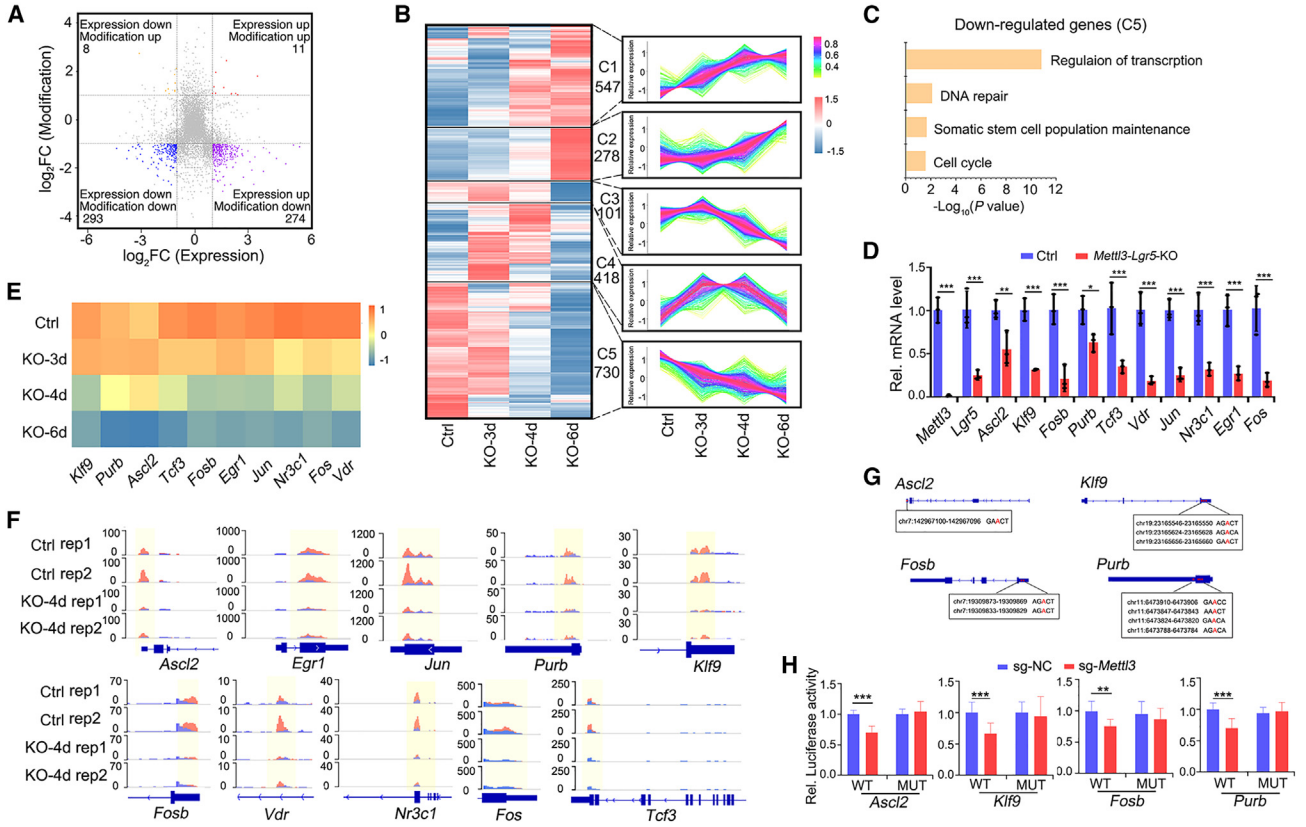

Figure 5. Identification of transcriptional factors that promote stemness

(A) Distribution of the genes that exhibited different m6A modification and gene expression levels in control or *Mettl3*-KO-GFP Lgr5^{high} cells ($|\log_2FC| \geq 1$; $p < 0.05$). The gene number in each category is shown.

(B) The expression of the genes with reduced m6A modification in *Mettl3*-KO-GFP Lgr5^{+} cells were divided into five modules according to their expression dynamics. The change trend in each module is shown in the line chart on the right.

(C) Functional enrichment analysis of the genes whose expression was downregulated at 3 dpt from the module C5 in (B).

(D) Expression of *Mettl3*, *Lgr5*, and the 10 TFs (*Ascl2*, *Klf9*, *Fosb*, *Purb*, *Tcf3*, *Vdr*, *Jun*, *Nr3c1*, *Egr1*, *Fos*) in FACS-sorted Lgr5^{high} cells from control and *Mettl3-Lgr5*-KO mice at 4 dpt by q-PCR. N = 3 mice per group.

(E) Expression heatmap of the 10 TF candidates in Lgr5^{+} ISCs from control and *Mettl3*-KO-GFP mice, based on bulk RNA-seq.

(F) Integrative Genomics Viewer (IGV) tracks displaying MeRIP-seq reads along the indicated mRNAs in Lgr5^{high} ISCs of control and *Mettl3*-KO-GFP mice. Blue reads are from input libraries and red reads from anti-m6A immunoprecipitation libraries. The y axis represents the CPM (count per million) of genes. The yellow boxes of the tracks depict the positions of m6A peaks.

(G) Representative m6A modification sites at the genomic loci of *Ascl2*, *Klf9*, *Fosb*, and *Purb*.

(H) Fetal human colon cells (FHC cells) were transfected with WT or MUT 3′ UTR luciferase reporter, as well as with control sgRNA or *Mettl3* sgRNA, and luciferase activity was determined 48 h later. NC: control. MUT: mutation all sites (A to T). Data from three independent experiments were combined and are shown. The data represent mean ± SD. ***$p < 0.001$, **$p < 0.01$, two-way ANOVA (D and H). See also Figure S6 and Tables S2–S4.

modification is critical for stabilization of *AKFP* transcripts, whose protein products then regulate stemness gene expression to maintain Lgr5^{+} ISCs.

DISCUSSION

In this study, we showed that the m6A methyltransferase *Mettl3* is essential for the homeostatic maintenance of the small intestinal epithelium. m6A modification has emerged as a crucial regulation in tissue development and stem cell fate determination (Batista et al., 2014; Cao et al., 2020; Geula et al., 2015; Yoon et al., 2017), while the overall impact of this modification on stem cells is complex (Cui et al., 2017; Vu et al., 2017; Wang et al., 2018; Weng et al., 2018; Zhang et al., 2017), due to diversified targets and different regulations on the targets. Several studies have reported the regulatory role of m6A modification in

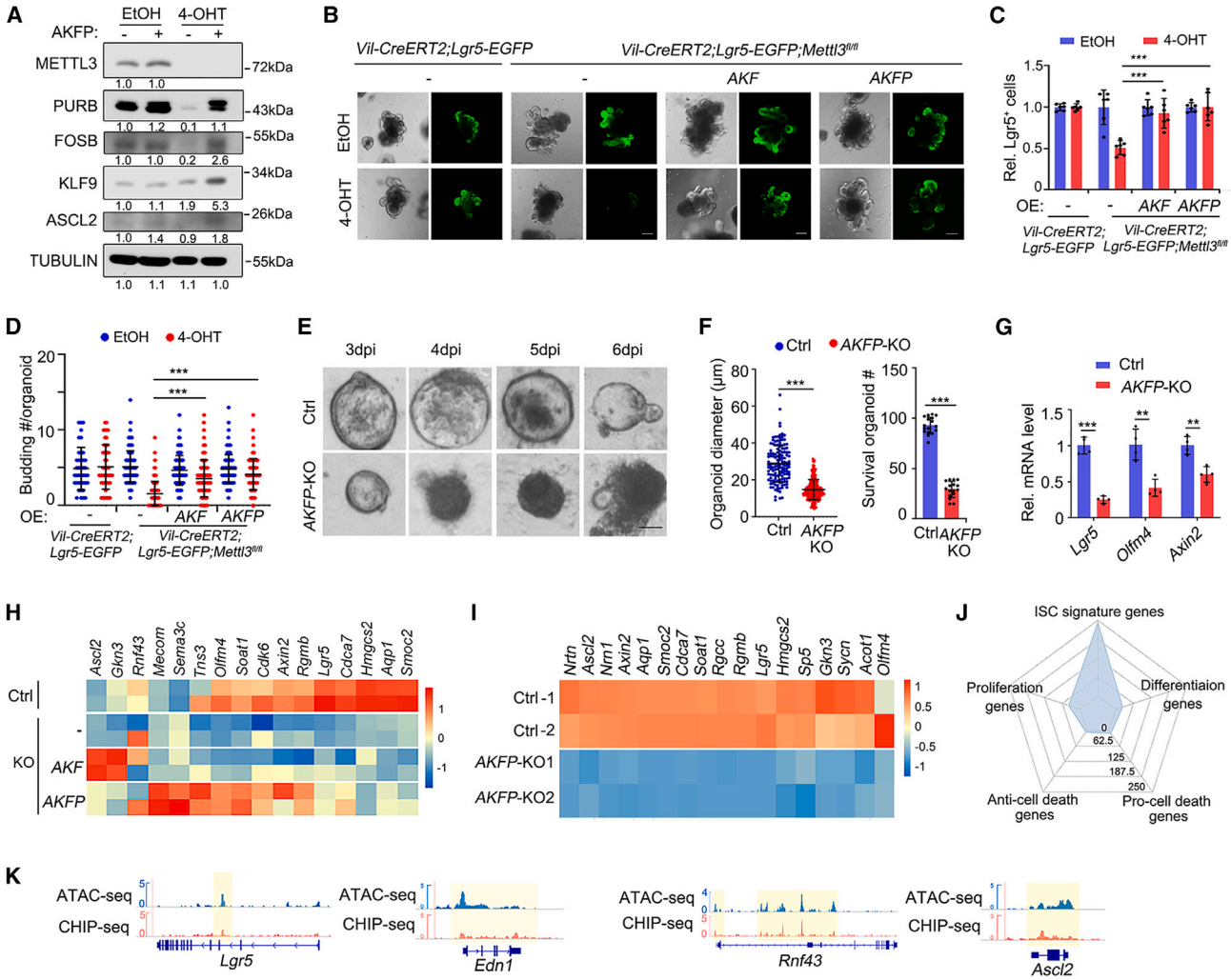

Figure 6. ASCL2, KLF9, FOSB, and PURB collaborate to regulate stemness gene expression

(A) Immunoblots of ASCL2, KLF9, FOSB, and PURB protein expression in organoids derived from the crypts of *Villin-CreERT2;Lgr5-EGFP-IRES-CreERT2;Mettl3*$^{fl/fl}$ mice infected with control retrovirus or AKFP-expressed retrovirus at day 5 after EtOH or 4-OHT treatment for 2 days. TUBULIN, loading control.

(B) Representative morphology and Lgr5^{+} cells of organoids derived from the crypts of *Villin-CreERT2;Lgr5-EGFP-IRES-CreERT2;Mettl3*$^{fl/fl}$ mice, which were infected with retrovirus expressing *AKF* (*Ascl2*, *Klf9*, and *Fosb*) or *AKFP* (*Ascl2*, *Klf9*, *Fosb*, and *Purb*) and then treated with EtOH or 4-OHT for 2 days and subjected for analysis at day 5.

(C and D) Relative Lgr5^{+} cell number (C) and budding number (D) of organoid in (A). Data from three independent experiments were combined and are shown (C). N > 100 organoids per group from three independent experiments (D).

(E) Representative morphology of organoids derived from the crypts of *Villin-CreERT2;Rosa26*$^{loxp\text{-}stop\text{-}loxp\text{-}Cas9\text{-}EGFP}$ mice at indicated times, which were infected with recombinant AAV to knock out *AKFP* or control recombinant AAV.

(F) Organoid diameter (left) of control or *AKFP*-KO organoid at day 3 and survival organoid number (right) at day 4. N > 100 organoids per group from four independent experiments.

(G) q-PCR shows gene expression of control and *AKFP*-KO organoids at day 4. Data from four independent experiments were combined and are shown.

(H and I) Stemness gene expression of *AKF* and *AKFP* overexpression organoids in (A) and *AKFP*-KO organoids in (E).

(J) Function characteristics distribution of all the predicted target genes of KLF9, ASCL2, FOSB, and PURB.

(K) ChIP-seq and ATAC-seq tracks of Fosb binding to the stem cell signature genes *Lgr5*, *Rnf43*, *Edn1*, *Ascl2*. The data represent mean ± SD. ***p < 0.001, **p < 0.01, two-way ANOVA (C, D, and G), unpaired two-tailed t test (F). Scale bar: 100 μm (A, E). *AKF*: *Ascl2*, *Klf9*, and *Fosb*; *AKFP*: *Ascl2*, *Klf9*, *Fosb*, and *Purb*. See also Figure S6 and Table S2.

the intestinal epithelium: METTL3-mediated m6A modification has been shown to promote colorectal cancer development by activating glycolysis (Shen et al., 2020), stabilizing *SOX2* mRNA (Li et al., 2019) or *CCNE2* mRNA (Zhu et al., 2020); the m6A reader YTHDF1 mediates Wnt-driven ISC maintenance during regeneration and tumorigenesis by enhancing the translation of TCF7L2 (Han et al., 2020). Here, we demonstrate that conditional KO of *Mettl3* in the intestinal epithelium results in rapid loss of Lgr5$^+$ ISCs, enhanced cell death, and mild effects on differentiation, but it has no influence on proliferation. Loss of Lgr5$^+$ ISCs is very likely due to loss of their stem cell identity and accelerated cell death.

Stem cells are capable of proliferation, self-maintenance, and differentiation toward mature cells. At the time point when the stemness markers in ISCs disappear upon *Mettl3* KO or *Mettl3 Lgr5*-KO, the proliferation genes still remain in both *Mettl3*-deficient ISCs and TA cells. Owing to the low labeling efficiency of *Lgr5-EGFP-IRES-CreERT2* mice (Barker, 2014; Sato et al., 2009), no significant change of differentiation genes was observed in *Mettl3-Lgr5*-KO mice, which is different from the phenotype of *Mettl3*-KO mice. However, we did observe the impaired stemness phenotype in the GFP-labeling cells, which co-expressed CreERT2, and as a result, *Mettl3* was deleted in these cells upon tamoxifen treatment. Our sc-RNA-seq analysis also showed that *Mettl3* deletion reduced the expression of stem cell signature genes but elevated expression of the genes related to proliferation and differentiation in the ISCs cluster. Previous studies have attempted to determine the stemness signature for embryonic stem cells and adult stem cells by comparison of transcriptional profiling between stem cells and differentiated cells (Cai et al., 2004; Ivanova et al., 2002; Munoz et al., 2012; Ramalho-Santos et al., 2002). However, those stem cell signatures contain many genes related to cell proliferation. We show here that the program to control stemness gene expression can be uncoupled from the one to regulate proliferation.

Furthermore, we identified four TFs (*Ascl2*, *Klf9*, *Fosb*, and *Purb*), whose mRNA is stabilized by METTL3-mediated m6A modification. m6A generally promotes mRNA degradation (Shi et al., 2019; Wang et al., 2014a, 2014b), but we found that loss of m6A modification was correlated with reduced levels of these TF transcripts. How m6A stabilizes mRNA is unclear: it could be due to inappropriate splicing, as being proposed that m6A modification can regulate gene expression by affecting alternative splicing (Xu et al., 2017). These four TFs control the expression of stemness genes but not proliferation genes in ISCs. Furthermore, AKFP-overexpressing organoids could maintain Lgr5-GFP$^+$ cells number but did not suppress cell death; it is most likely that the m6A-modified death genes are not regulated by AKFP. It would be worthwhile to explore the mechanism underlying the m6A disruption-triggered cell death in the future. Our findings that the stemness program can be uncoupled from the proliferation program in ISCs also imply that similar mechanisms may also exist in other types of stem cells.

EXPERIMENTAL PROCEDURES

Resource availability

Corresponding author

Ye-Guang Chen (ygchen@tsinghua.edu.cn).

Material availability

All reagents generated in this study are available from the corresponding author.

Mice

Lgr5-EGFP-IRES-CreERT2 mice were obtained from the Jackson Laboratory. *Villin-CreERT2* mice were obtained from Dr. Sylvie Robine (Institute Curie-CNRS, Paris), *Mettl3*$^{fl/fl}$ mice from Dr. Wei Li (Institute of Zoology, CAS), *Lgr5-CreERT2* and *Rosa26*$^{loxp\text{-}stop\text{-}loxp\text{-}ZsGreen}$ mice from Dr. Xiao-Dong Wang (National Institute of Biological Sciences, Beijing), and *Rosa26*$^{loxp\text{-}stop\text{-}loxp\text{-}Cas9\text{-}EGFP}$ mice from Dr. Jianwei Wang (Tsinghua University). All mice were performed as previously described (Qi et al., 2017). For *Mettl3-KO*, *Mettl3*$^{fl/fl}$ mice were crossed with *Villin-CreERT2* mice. The *Vil-CreERT2;Mettl3*$^{fl/fl}$ mice and littermate mice (*Mettl3*$^{fl/fl}$) were intraperitoneally injected with four consecutive daily doses of 20 mg/mL tamoxifen (TAM) (Sigma, T5648-5G) in sunflower oil. To monitor the Lgr5-GFP$^+$ ISCs, the littermate mice, whose genotypes were *Villin-CreERT2;Lgr5-EGFP-IRES-CreERT2;Mettl3*$^{fl/fl}$, were treated with oil or tamoxifen, as control and *Mettl3*-KO-GFP, respectively. For *Mettl3-Lgr5*-KO, the littermate mice, whose genotypes were *Lgr5-EGFP-IRES-CreERT2;Mettl3*$^{w/w}$ or *Lgr5-EGFP-IRES-CreERT2;Mettl3*$^{fl/fl}$, were injected with tamoxifen for 5 days, as control and *Mettl3-Lgr5*-KO, respectively. For lineage tracing, control (*Lgr5-CreERT2;Rosa26*$^{loxp\text{-}stop\text{-}loxp\text{-}ZsGreen}$) mice and *Mettl3*$^{\Delta Lgr5}$ (*Mettl3*$^{fl/fl}$; *Lgr5-CreERT2;Rosa26*$^{loxp\text{-}stop\text{-}loxp\text{-}ZsGreen}$) mice were intraperitoneally injected with a single dose of 20 mg/mL TAM. The animals used in this study are summarized in Table S1.All animal studies were performed in accordance with the relevant guidelines and under the approval of the Institutional Animal Care and Use Committee of Tsinghua University.

Intestinal crypt and Lgr5$^+$ ISC isolation and organoids culture

Intestinal crypts were isolated and cultured as previously described (Qi et al., 2017). Briefly, the enriched intestinal crypts were isolated and embedded in Matrigel and seeded on plate. The ENR medium (advanced DMEM/F12 supplemented with penicillin/streptomycin, GlutaMAX, N2, B27, and *N*-acetylcysteine containing 50 ng/mL EGF, 100 ng/mL Noggin, and 500 ng/mL R-spondin1) was added and refreshed every 2 days.

To purify single Lgr5$^+$ cells, isolated intestinal crypts were treated with TrypLE (Gibco, 12604021). After passing through a 40-μm cell strainer (BD, 352340), staining with propidium iodide (Sigma, P4170), Lgr5$^+$ cells were sorted using MoFlo Astrios EQ (BeckMan). Lgr5$^+$ cells were embedded in Matrigel and seeded on a 48-well plate. The cells were cultured with expansion medium (ENR medium plus 6.67 μM blebbistatin, 2.5 μM CHIR-99021, 10% Wnt3a conditional medium) plus 1 μM Jagged1 (Zhang et al., 2020).

Virus production and organoid infection

Retrovirus and recombinant adeno-associated virus (AAV) were produced as previously described (Koo et al., 2011; Li et al., 2021). Before virus infection, organoids were cultured with the expansion medium plus 10 mM nicotinamide for 2 days. Then, the organoids were digested with TrypLE (Gibco, 12604021) and re-suspended with the expansion medium plus 10 μg/mL polybrene (Macgene, MC032) containing virus. We added 250 μL of expansion medium plus polybrene containing cells and virus on the pre-solidified Matrigel and incubated overnight at 37°C. The next day, we removed the medium and washed the virus with warm PBS. Then, we overlaid 10 μL Matrigel and cultured the organoids with expansion medium.

For retrovirus infection, we changed the medium with ENR plus 2 μg/mL puromycin 2 days post-infection. After the organoids grew normally under the puromycin selection, protein expression was induced with 4-OHT (0.5 μM, Sigma, H7904). For recombinant AAV, *Villin-CreERT2;Rosa26*$^{loxp\text{-}stop\text{-}loxp\text{-}Cas9\text{-}EGFP}$ organoids were pretreated with 4-OHT to induce Cas9 expression.

Immunoblotting

Cells were lysed in RIPA buffer (Beyotime, P0013B) with protease inhibitors (Roche, 04693132001) and PMSF (Beyotime, ST506). After quantification using a BCA protein assay kit (Beyotime, P0012S), 40 μg of total protein was separated with 7.5% SDS-PAGE under denaturing conditions and was transferred to nitrocellulose membranes (PALL, 66485). The membranes were blocked and then incubated with the primary antibody overnight at 4°C, followed by incubation with anti-rabbit or anti-mouse conjugated antibodies. Antibodies are listed in the supplemental experimental procedures.

Immunofluorescence and histological staining

Immunofluorescence and histological staining were performed as previously described (Qi et al., 2017). H&E staining was performed according to the manufacturer instructions (Beyotime, C0205S). Briefly, the sections were dewaxed by conventional procedures and stained with hematoxylin for 2 min and eosin for 20 s. Alcian blue staining was used to detect goblet cells, and slides were stained with Alcian blue for 15 min and nuclear fast red for 1 min (Baso, BA4087B). All sections were visualized with a confocal microscope (Olympus, FV3000) or a slide scanning system (Jiang Feng, KF-PRO-120).

Terminal deoxynucleotidyl transferase-mediated dUTP nick end labeling assay

Paraformaldehyde-fixed paraffin-embedded tissues were subjected to cell death assessment using the *In Situ* Cell Death detection kit (Roche, 11684795910).

Organoid time-lapse imaging

To mark the cell membrane, 1.25 μg/mL CellMask Orange Plasma Membrane Stain (Thermo Fisher Scientific, C10045) was added to the medium 12 h before imaging. Confocal time-lapse imaging was performed with Nikon AX R Confocal Microscope System by resonant scanner and Nikon NIS-Elements Denoise.ai software. Different organoids were selected and imaged every 1 h from day 4.5 to day 6.5. A volume of 200–300 μm was gained every 3 μm along the z axis. To exclude autofluorescence of dead cells, only organoids containing clear buds were selected to build surfaces for statistics. Surfaces at different times marking Lgr5-GFP signals, value of fluorescence intensity, and surface volume were computed automatically by the Imaris software at the same parameters. The average fluorescence intensity value was calculated as the total fluorescence intensity at each time point divided by the surface volume at the starting point.

BrdU and EdU labeling

Mice were given a single intraperitoneal injection of 100 μL BrdU (BD Pharmingen BrdU Flow Kits, BD, 552598) 2 or 24 h before intestine isolation. BrdU staining was performed with the BrdU flow kit (BD Pharmingen). For cell cycle analysis, the epithelium was stained with EpCam-PE, BrdU-APC, and 7-AAD 2 h later after a single intraperitoneal injection of BrdU. Cell cycle was analyzed by FACS. EdU labeling was performed by following the manufacturer's instruction (Click-iT EdU Imaging Kit, Invitrogen, C10339).

RNA extraction and quantitative RT-PCR (q-PCR)

Total RNA from tissue or sorted cells was extracted with RNeasy Mini Kit (QIAGEN, 74104) or TRIzol Reagent (Thermo Fisher Scientific, 15596026), respectively. RNA was reverse-transcribed into cDNA using ReverTra Ace-α kit (TOYOBO, FSK-101). q-PCR was carried out with NovoStart SYBR qPCR Super-Mix Plus (Novoprotein, E096-01A) on LightCycle 480II PCR system (Roche). All primer sequences are shown in Table S2 and were purchased from Sangon Biotech.

RNA-seq

Total RNA was extracted with RNeasy Mini Kit (QIAGEN) according to the manufacturer's instructions. Bulk RNA-seq was performed using the Illumina Hiseq X Ten and analyzed as previously described (Pertea et al., 2016).

MeRIP-seq

Total RNA was extracted with RNeasy Mini Kit (QIAGEN, 74104). mRNA was purified using Dynabeads mRNA Purification kit (Invitrogen, 61006). Purified mRNA was fragmented into ~100 nucleotides by RNA Fragmentation Reagents (Ambion, AM8740) and immunoprecipitation with m6A antibody (NEB, E1610S), followed by RNA extraction using RNA clean&concentrator-5 (ZYMO RESEARCH, 1013). Data analysis is described in the supplemental experimental procedures in detail.

ATAC-seq

For mini-ATAC-seq, the library was constructed with TruePrep DNA library Prep Kit V2 for Illumina (Vazyme, TD 202 and TD502). Subsequently, the library was purified with AMPure XP beads (Beckman, A63881) and sequenced with Illumina Novaseq 6000. HISAT2 was used to align the sequences to the mouse genome and generate bam files. After being deprived of PCR duplicates using Picard tools, Deeptools (3.3.1) bamCoverage was used to generate bigwig files from bam files. MACS2 (v2.2.5) was used for peak calling and to generate bed files from aligned reads.

scRNA-seq

Single-cell suspensions from the intestinal epithelium of *Mettl3*-KO-GFP-4d and control mice were sorted by FACS and re-suspended at a density of 1,000 cells per μL (n = 3 mice per group). About 8,000 cells were loaded into each reaction. RNA transcripts from single cells were uniquely barcoded and reverse-transcribed. scRNA-seq libraries were generated using the Chromium Single Cell 3′ Reagent Ki V3 (10× Genomics). The libraries were sequenced as paired-end with Illumina Novaseq 6000.

Raw reads were aligned to the GRCm38/mm10 mouse genome, and Cell Ranger (v3.1.0) was used to estimate unique molecular

identifiers. Raw aligned features were loaded and processed using the Seurat package (v4.0.2) in R version 4.0.5. Low-quality cells were filtered if they expressed no more than 200 genes or with more than 20% of mitochondrial genes. More bioinformation analysis is described in the supplemental experimental procedures.

Dual luciferase reporter assay

The 3′ UTR fragments of Ascl2, Fosb, Klf9, and Purb containing enriched m6A motif (RRACH) and their respective A-to-T mutant fragments were cloned into pGL3-CMV firefly luciferase vector. FHCs (fetal human colon cells) were seeded and co-transfected with pGL3-CMV-WT-3′UTR or pGL3-CMV-mut-3′UTR, Renilla luciferase plasmid, and px458-sgNC/Mettl3-1 using Lipo2000 (Invitrogen, 11668019). The relative luciferase activity was determined using the Dual-Luciferase Reporter Assay System and Microplate Chemiluminescence Meter (Berthold, LB960) 48 h later. The sequences are shown in Tables S3 and S4.

Statistical analysis

All experiments were carried out with at least three independent experiments. Exact numbers of mice, fields, and organoids are shown in the figure legends. Statistical analysis was performed with Graphpad Prism v8.0. All data shown in graphs represent mean ± SD as indicated in the figure legends. Unpaired two-tailed t test, one-way ANOVA, two-way ANOVA, and Log rank test were used to compare differences, as indicated in the figure legends.

Data and code availability

The RNA-seq data, scRNA-seq data, MeRIP-seq data, ATAC-seq data, and ChIP-seq data generated in this study are publicly available through the Gene Expression Omnibus (GEO) with the accession code GSE186917. The scRNA-seq data GSE148693 was used to confirm the 23 stem genes (Gu et al., 2021). All codes that enable the main steps of the analysis and data are available from the corresponding author under request.

SUPPLEMENTAL INFORMATION

Supplemental information can be found online at https://doi.org/10.1016/j.stemcr.2023.03.007.

AUTHOR CONTRIBUTIONS

Y.L., M.H., X.W., and Y.-G.C conceived the experiments and wrote the manuscript. Y.L., M.H., Z.L., and S.L. performed the experiments, and X.W. analyzed the data.

ACKNOWLEDGMENTS

We thank Drs. Sylvie Robine, Wei Li, Xiao-Dong Wang, and Jianwei Wang for mice, Dr. Wei Xie for the advice on ATAC-seq, and Dr. Meng Xu and Dr. Yun-Gui Yang for the advice on MeRIP-seq. We are grateful to Mengxian Zhang and Huidong Liu for critical comments and valuable review. This work was supported by grants from the National Key Research and Development Program of China (2017YFA0103601) and the National Natural Science Foundation of China (31988101 and 31730056 to Y.G.C.; 31900550 to Y.L.).

CONFLICT OF INTERESTS

The authors declare no competing financial interests.

Received: July 4, 2022
Revised: March 8, 2023
Accepted: March 13, 2023
Published: April 6, 2023

REFERENCES

Barker, N. (2014). Adult intestinal stem cells: critical drivers of epithelial homeostasis and regeneration. Nat. Rev. Mol. Cell Biol. *15*, 19–33. https://doi.org/10.1038/nrm3721.

Batista, P.J., Molinie, B., Wang, J., Qu, K., Zhang, J., Li, L., Bouley, D.M., Lujan, E., Haddad, B., Daneshvar, K., et al. (2014). m(6)A RNA modification controls cell fate transition in mammalian embryonic stem cells. Cell Stem Cell *15*, 707–719. https://doi.org/10.1016/j.stem.2014.09.019.

Cai, J., Weiss, M.L., and Rao, M.S. (2004). In search of "stemness". Exp. Hematol. *32*, 585–598. https://doi.org/10.1016/j.exphem.2004.03.013.

Cao, Y., Zhuang, Y., Chen, J., Xu, W., Shou, Y., Huang, X., Shu, Q., and Li, X. (2020). Dynamic effects of Fto in regulating the proliferation and differentiation of adult neural stem cells of mice. Hum. Mol. Genet. *29*, 727–735. https://doi.org/10.1093/hmg/ddz274.

Clevers, H. (2013). The intestinal crypt, a prototype stem cell compartment. Cell *154*, 274–284. https://doi.org/10.1016/j.cell.2013.07.004.

Cui, Q., Shi, H., Ye, P., Li, L., Qu, Q., Sun, G., Sun, G., Lu, Z., Huang, Y., Yang, C.G., et al. (2017). m(6)A RNA methylation regulates the self-renewal and tumorigenesis of glioblastoma stem cells. Cell Rep. *18*, 2622–2634. https://doi.org/10.1016/j.celrep.2017.02.059.

Deng, X., Su, R., Weng, H., Huang, H., Li, Z., and Chen, J. (2018). RNA N(6)-methyladenosine modification in cancers: current status and perspectives. Cell Res. *28*, 507–517. https://doi.org/10.1038/s41422-018-0034-6.

Geula, S., Moshitch-Moshkovitz, S., Dominissini, D., Mansour, A.A., Kol, N., Salmon-Divon, M., Hershkovitz, V., Peer, E., Mor, N., Manor, Y.S., et al. (2015). Stem cells. m6A mRNA methylation facilitates resolution of naive pluripotency toward differentiation. Science *347*, 1002–1006. https://doi.org/10.1126/science.1261417.

Gu, W., Wang, H., Huang, X., Kraiczy, J., Singh, P.N.P., Ng, C., Dagdeviren, S., Houghton, S., Pellon-Cardenas, O., Lan, Y., et al. (2021). SATB2 preserves colon stem cell identity and mediates ileum-colon conversion via enhancer remodeling. Cell Stem Cell *29*, 101–115.e10. https://doi.org/10.1016/j.stem.2021.09.004.

Han, B., Yan, S., Wei, S., Xiang, J., Liu, K., Chen, Z., Bai, R., Sheng, J., Xu, Z., and Gao, X. (2020). YTHDF1-mediated translation amplifies Wnt-driven intestinal stemness. EMBO Rep. *21*, e49229. https://doi.org/10.15252/embr.201949229.

He, P.C., and He, C. (2021). m(6) A RNA methylation: from mechanisms to therapeutic potential. EMBO J. *40*, e105977. https://doi.org/10.15252/embj.2020105977.

Ivanova, N.B., Dimos, J.T., Schaniel, C., Hackney, J.A., Moore, K.A., and Lemischka, I.R. (2002). A stem cell molecular signature. Science *298*, 601–604. https://doi.org/10.1126/science.1073823.

Koo, B.K., Stange, D.E., Sato, T., Karthaus, W., Farin, H.F., Huch, M., van Es, J.H., and Clevers, H. (2011). Controlled gene expression in primary Lgr5 organoid cultures. Nat. Methods *9*, 81–83. https://doi.org/10.1038/nmeth.1802.

Li, F., Huang, Q., Chen, J., Peng, Y., Roop, D.R., Bedford, J.S., and Li, C.Y. (2010). Apoptotic cells activate the "phoenix rising" pathway to promote wound healing and tissue regeneration. Sci. Signal. *3*, ra13. https://doi.org/10.1126/scisignal.2000634.

Li, T., Hu, P.S., Zuo, Z., Lin, J.F., Li, X., Wu, Q.N., Chen, Z.H., Zeng, Z.L., Wang, F., Zheng, J., et al. (2019). METTL3 facilitates tumor progression via an m(6)A-IGF2BP2-dependent mechanism in colorectal carcinoma. Mol. Cancer *18*, 112. https://doi.org/10.1186/s12943-019-1038-7.

Li, Y., He, Y., Peng, J., Su, Z., Li, Z., Zhang, B., Ma, J., Zhuo, M., Zou, D., Liu, X., et al. (2021). Mutant Kras co-opts a proto-oncogenic enhancer network in inflammation-induced metaplastic progenitor cells to initiate pancreatic cancer. Nat. Cancer *2*, 49–65. https://doi.org/10.1038/s43018-020-00134-z.

Liu, Y., and Chen, Y.G. (2020). Intestinal epithelial plasticity and regeneration via cell dedifferentiation. Cell Regen. *9*, 14. https://doi.org/10.1186/s13619-020-00053-5.

Muñoz, J., Stange, D.E., Schepers, A.G., van de Wetering, M., Koo, B.K., Itzkovitz, S., Volckmann, R., Kung, K.S., Koster, J., Radulescu, S., et al. (2012). The Lgr5 intestinal stem cell signature: robust expression of proposed quiescent '+4' cell markers. EMBO J. *31*, 3079–3091. https://doi.org/10.1038/emboj.2012.166.

Pertea, M., Kim, D., Pertea, G.M., Leek, J.T., and Salzberg, S.L. (2016). Transcript-level expression analysis of RNA-seq experiments with HISAT, StringTie and Ballgown. Nat. Protoc. *11*, 1650–1667. https://doi.org/10.1038/nprot.2016.095.

Post, Y., and Clevers, H. (2019). Defining adult stem cell function at its simplest: the ability to replace lost cells through mitosis. Cell Stem Cell *25*, 174–183. https://doi.org/10.1016/j.stem.2019.07.002.

Qi, Z., and Chen, Y.G. (2015). Regulation of intestinal stem cell fate specification. Sci. China Life Sci. *58*, 570–578. https://doi.org/10.1007/s11427-015-4859-7.

Qi, Z., Li, Y., Zhao, B., Xu, C., Liu, Y., Li, H., Zhang, B., Wang, X., Yang, X., Xie, W., et al. (2017). BMP restricts stemness of intestinal Lgr5(+) stem cells by directly suppressing their signature genes. Nat. Commun. *8*, 13824. https://doi.org/10.1038/ncomms13824.

Ramalho-Santos, M., Yoon, S., Matsuzaki, Y., Mulligan, R.C., and Melton, D.A. (2002). "Stemness": transcriptional profiling of embryonic and adult stem cells. Science *298*, 597–600. https://doi.org/10.1126/science.1072530.

Sato, T., Vries, R.G., Snippert, H.J., van de Wetering, M., Barker, N., Stange, D.E., van Es, J.H., Abo, A., Kujala, P., Peters, P.J., and Clevers, H. (2009). Single Lgr5 stem cells build crypt-villus structures in vitro without a mesenchymal niche. Nature *459*, 262–265. https://doi.org/10.1038/nature07935.

Shen, C., Xuan, B., Yan, T., Ma, Y., Xu, P., Tian, X., Zhang, X., Cao, Y., Ma, D., Zhu, X., et al. (2020). m(6)A-dependent glycolysis enhances colorectal cancer progression. Mol. Cancer *19*, 72. https://doi.org/10.1186/s12943-020-01190-w.

Shi, H., Wei, J., and He, C. (2019). Where, when, and how: context-dependent functions of RNA methylation writers, readers, and erasers. Mol. Cell *74*, 640–650. https://doi.org/10.1016/j.molcel.2019.04.025.

Tirosh, I., Izar, B., Prakadan, S.M., Wadsworth, M.H., 2nd, Treacy, D., Trombetta, J.J., Rotem, A., Rodman, C., Lian, C., Murphy, G., et al. (2016). Dissecting the multicellular ecosystem of metastatic melanoma by single-cell RNA-seq. Science *352*, 189–196. https://doi.org/10.1126/science.aad0501.

Vogel, G. (2003). Stem cells. 'Stemness' genes still elusive. Science *302*, 371. https://doi.org/10.1126/science.302.5644.371a.

Vu, L.P., Pickering, B.F., Cheng, Y., Zaccara, S., Nguyen, D., Minuesa, G., Chou, T., Chow, A., Saletore, Y., MacKay, M., et al. (2017). The N(6)-methyladenosine (m(6)A)-forming enzyme METTL3 controls myeloid differentiation of normal hematopoietic and leukemia cells. Nat. Med. *23*, 1369–1376. https://doi.org/10.1038/nm.4416.

Wang, X., Lu, Z., Gomez, A., Hon, G.C., Yue, Y., Han, D., Fu, Y., Parisien, M., Dai, Q., Jia, G., et al. (2014a). N6-methyladenosine-dependent regulation of messenger RNA stability. Nature *505*, 117–120. https://doi.org/10.1038/nature12730.

Wang, Y., Chiang, I.L., Ohara, T.E., Fujii, S., Cheng, J., Muegge, B.D., Ver Heul, A., Han, N.D., Lu, Q., Xiong, S., et al. (2019). Long-term culture captures injury-repair cycles of colonic stem cells. Cell *179*, 1144–1159.e15. https://doi.org/10.1016/j.cell.2019.10.015.

Wang, Y., Li, Y., Toth, J.I., Petroski, M.D., Zhang, Z., and Zhao, J.C. (2014b). N6-methyladenosine modification destabilizes developmental regulators in embryonic stem cells. Nat. Cell Biol. *16*, 191–198. https://doi.org/10.1038/ncb2902.

Wang, Y., Li, Y., Yue, M., Wang, J., Kumar, S., Wechsler-Reya, R.J., Zhang, Z., Ogawa, Y., Kellis, M., Duester, G., and Zhao, J.C. (2018). N(6)-methyladenosine RNA modification regulates embryonic neural stem cell self-renewal through histone modifications. Nat. Neurosci. *21*, 195–206. https://doi.org/10.1038/s41593-017-0057-1.

Weng, H., Huang, H., Wu, H., Qin, X., Zhao, B.S., Dong, L., Shi, H., Skibbe, J., Shen, C., Hu, C., et al. (2018). METTL14 inhibits hematopoietic stem/progenitor differentiation and promotes leukemogenesis via mRNA m(6)A modification. Cell Stem Cell *22*, 191–205.e9. https://doi.org/10.1016/j.stem.2017.11.016.

Xu, K., Yang, Y., Feng, G.H., Sun, B.F., Chen, J.Q., Li, Y.F., Chen, Y.S., Zhang, X.X., Wang, C.X., Jiang, L.Y., et al. (2017). Mettl3-mediated m(6)A regulates spermatogonial differentiation and meiosis initiation. Cell Res. *27*, 1100–1114. https://doi.org/10.1038/cr.2017.100.

Yoon, K.J., Ringeling, F.R., Vissers, C., Jacob, F., Pokrass, M., Jimenez-Cyrus, D., Su, Y., Kim, N.S., Zhu, Y., Zheng, L., et al. (2017). Temporal control of mammalian cortical neurogenesis by m(6)A methylation. Cell *171*, 877–889.e17. https://doi.org/10.1016/j.cell.2017.09.003.

Zaccara, S., Ries, R.J., and Jaffrey, S.R. (2019). Reading, writing and erasing mRNA methylation. Nat. Rev. Mol. Cell Biol. *20*, 608–624. https://doi.org/10.1038/s41580-019-0168-5.

Zhang, C., Chen, Y., Sun, B., Wang, L., Yang, Y., Ma, D., Lv, J., Heng, J., Ding, Y., Xue, Y., et al. (2017). m(6)A modulates haematopoietic stem and progenitor cell specification. Nature *549*, 273–276. https://doi.org/10.1038/nature23883.

Zhang, M., Liu, Y., and Chen, Y.G. (2020). Generation of 3D human gastrointestinal organoids: principle and applications. Cell Regen. *9*, 6. https://doi.org/10.1186/s13619-020-00040-w.

Zhu, G., Hu, J., and Xi, R. (2021). The cellular niche for intestinal stem cells: a team effort. Cell Regen. *10*, 1. https://doi.org/10.1186/s13619-020-00061-5.

Zhu, W., Si, Y., Xu, J., Lin, Y., Wang, J.Z., Cao, M., Sun, S., Ding, Q., Zhu, L., and Wei, J.F. (2020). Methyltransferase like 3 promotes colorectal cancer proliferation by stabilizing CCNE1 mRNA in an m6A-dependent manner. J. Cell Mol. Med. *24*, 3521–3533. https://doi.org/10.1111/jcmm.15042.

Stem Cell Reports, Volume *18*

Supplemental Information

Segregation of the stemness program from the proliferation program in intestinal stem cells

Yuan Liu, Meimei Huang, Xiaodan Wang, Zinan Liu, Siqi Li, and Ye-Guang Chen

Fig S1

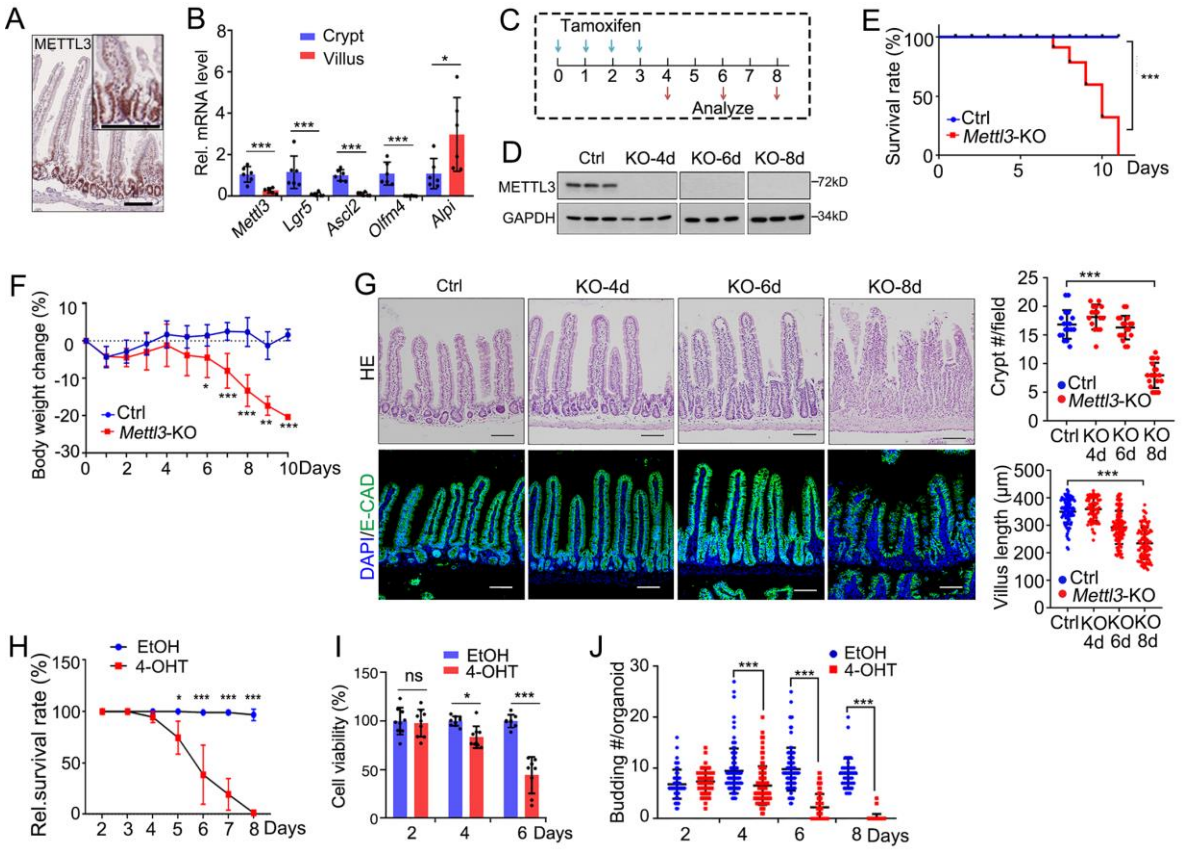

Figure S1. *Mettl3* is required for small intestine maintenance, related to Figure 1.

(A) Immunohistochemical staining of METTL3 in the jejunum. (B) q-PCR analysis of *Mettl3*, *Lgr5*, *Ascl2*, *Olfm4* and *Alpi* gene expression in jejunum crypt and villus. N=6 mice. (C) Schematic of tamoxifen treatment regimen and analysis of tissues from control (*Mettl3*$^{fl/fl}$) and *Mettl3*-KO (*Villin-CreERT2;Mettl3*$^{fl/fl}$) mice after tamoxifen (TAM) injection at the indicated time. (D) Immunoblot of METTL3 protein expression in intestinal crypt epithelium isolated from control (*Mettl3*$^{fl/fl}$) and *Mettl3*-KO mice (*Villin-CreERT2;Mettl3*$^{fl/fl}$) at indicated time after TAM injection. GAPDH, loading control. N=3 mice/group. (E) Survival plot for control (*Mettl3*$^{fl/fl}$) and *Mettl3*-KO (*Villin-CreERT2;Mettl3*$^{fl/fl}$) mice of 8-10 weeks old after injected with 20 mg/mL TAM for 4 days. N=11 mice/group. (F) Body weight following TAM injection of control (*Mettl3*$^{fl/fl}$) and *Mettl3*-KO (*Villin-CreERT2;Mettl3*$^{fl/fl}$) mice. N=9 mice/group. (G) Representative hematoxylin and eosin (HE) and immunofluorescence staining of the jejunum from control (*Mettl3*$^{fl/fl}$) and *Mettl3*-KO (*Villin-CreERT2;Mettl3*$^{fl/fl}$) mice at the indicated time after first TAM injection. Crypt number and villus length were shown in the right. N=3 mice/group, n=5 fields/mouse, n>100 villi/group. (H-J) Survival rate (H), cell viability (I) and budding number (J) in the organoids derived from *Mettl3*$^{fl/fl}$*;Villin-CreERT2* mice at the indicated time following EtOH or 4-hydroxytamoxifen (4-OHT) treatment for 2 days. N>100 organoids/group from three independent experiments. Nuclei were counter-stained with DAPI. The data represent mean±SD. *** P<0.001, ** P<0.01, * P<0.05, one-way ANOVA (G), two-way ANOVA (B, F, H, I and J), Log-rank test (E). Scale bars: 100 μm (A and G).

Fig S2

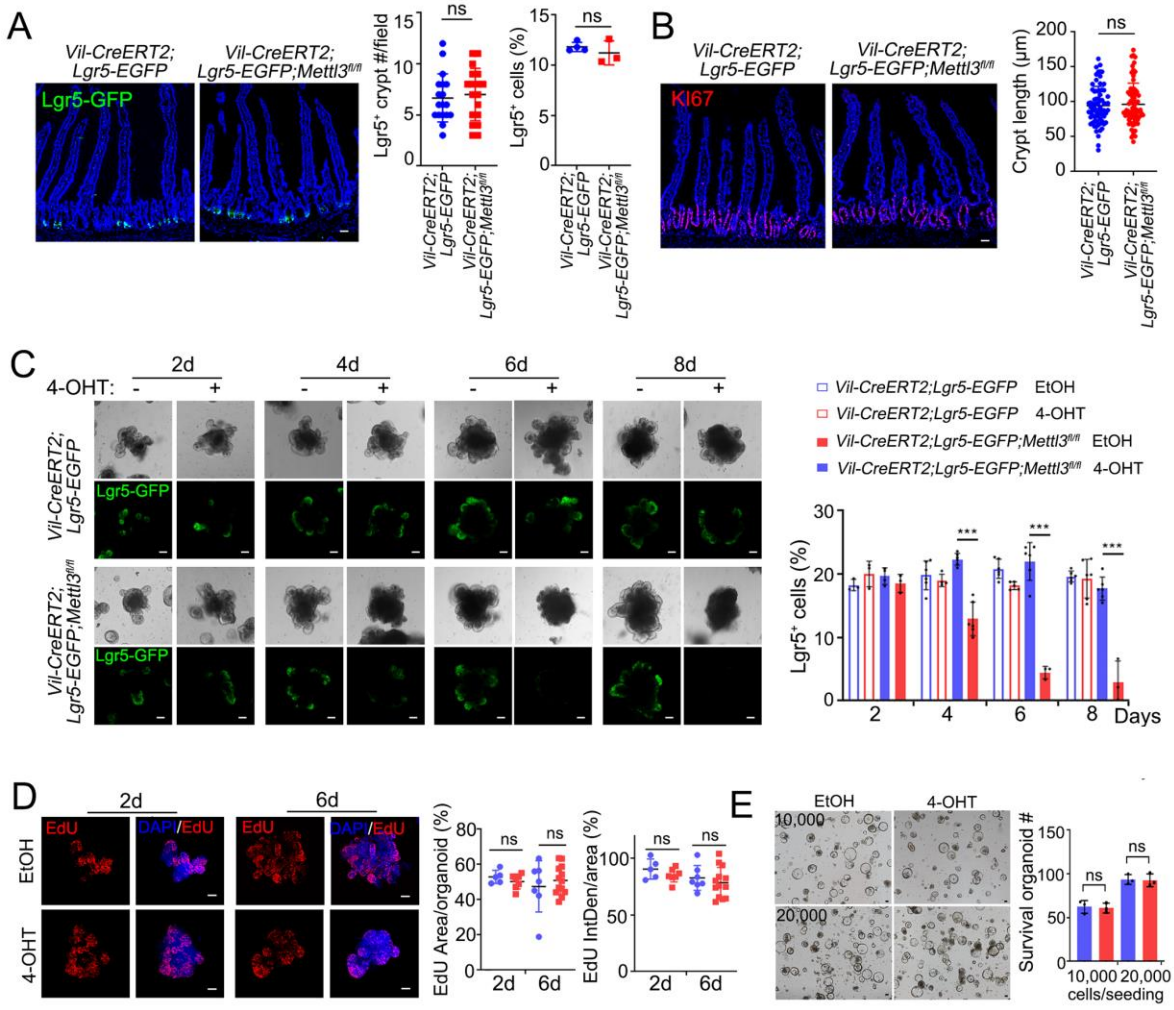

Figure S2. *Mettl3* is required for the development and maintenance of small intestine, related to Figure 1 and 2.

(A, B) Representative images and quantification of Lgr5-GFP$^+$ cells and KI67$^+$ cells in the jejunum of mice at 6 dpt. *Vil-CreERT2;Lgr5-EGFP* and *Vil-CreERT2;Lgr5-EGFP;Mettl3$^{fl/fl}$* mice were treated with TAM and oil, respectively. N=3 mice/group. (C) Representative images and quantification of Lgr5-GFP$^+$ cells in organoid derived from *Vil-CreERT2;Lgr5-EGFP* and *Vil-CreERT2;Lgr5-EGFP;Mettl3$^{fl/fl}$* mice after EtOH or 4-OHT treatment. Data from three independent experiments were combined and shown. (D) Representative images and quantification of EdU$^+$ cells in organoid derived from *Vil-CreERT2;Lgr5-EGFP* mice at 2 or 6 dpt. N=5-13 organoids/group from three independent experiments. (E) Representative images (left) and quantification (right) of intestinal organoids cultured from sorted Lgr5-GFP$^+$ cells derived from *Lgr5-EGFP-IRES-CreERT2;Mettl3$^{w/w}$* mice after treated with EtOH or 4-OHT for 5 days. The number of seeded cells was 10,000 and 20,000. Data from three independent experiments were combined and shown. Nuclei were counter-stained with DAPI. The data represent mean±SD. *** P<0.001, ** P<0.01, * P<0.05, unpaired two-tailed t-test (A, B), two-way ANOVA (C, D and E). Scale bars: 50 μm (A-E).

Fig S3

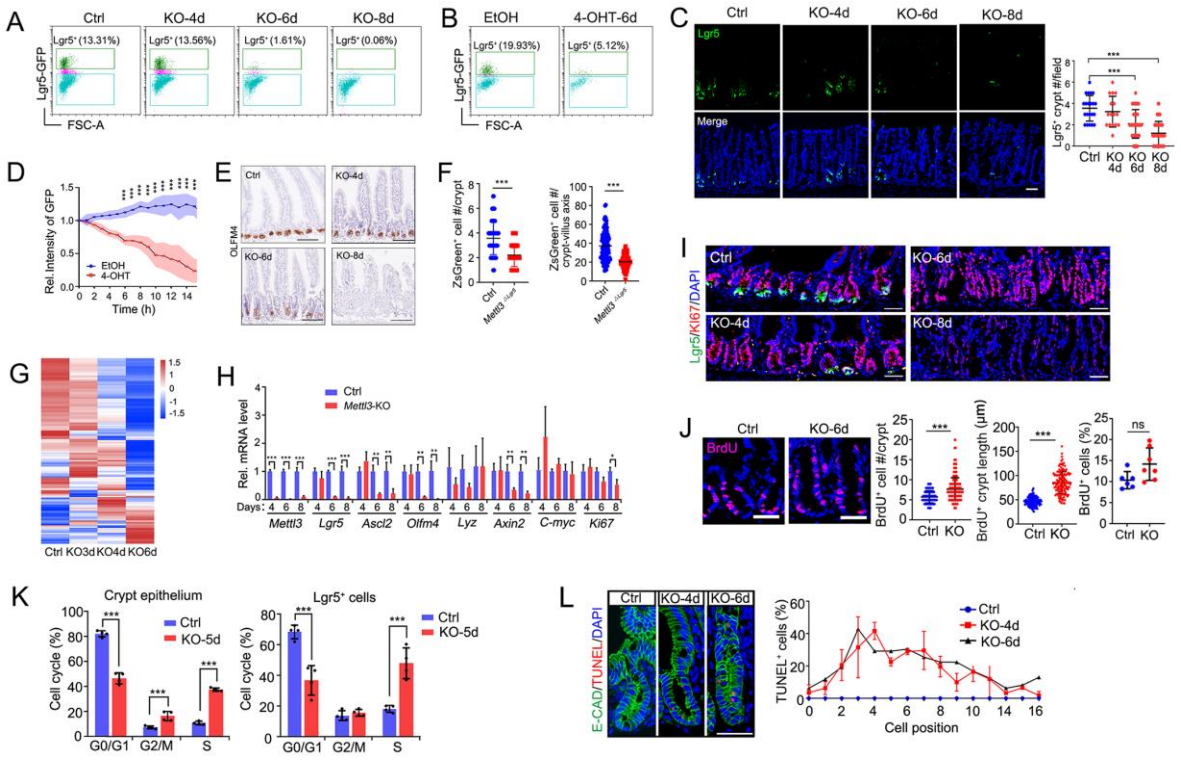

Figure S3. *Mettl3* deletion leads to loss of intestinal stem cells, hyper-proliferation and cell death in crypts, related to Figure 1.

(A) Lgr5-GFP^{+} cells in the crypts from control and *Mettl3*-KO-GFP mice at the indicated time, as revealed by FACS. (B) Lgr5-GFP^{+} cells of the organoids derived from *Vil-CreERT2;Lgr5-EGFP-IRES-CreERT2;Mettl3$^{fl/fl}$* mice at day 6 after treated with EtOH or 4-OHT for 2 days. (C) Representative images and quantification of Lgr5-GFP^{+} stem cells in the colon of control and *Mettl3*-KO-GFP mice at the indicated time after TAM injection. N=3 mice/group, n=5-10 fields/mouse. (D) Quantification of relative average fluorescence intensity of Lgr5-GFP at 1h intervals at day 4.5 after EtOH or 4-OHT treatment for 2 days, as revealed by confocal microscopy. N=5 organoids/group from three independent experiments. (E) Immunohistochemical staining of OLFM4 in the jejunum of control (*Mettl3$^{fl/fl}$*) and *Mettl3*-KO (*Vil-CreERT2;Mettl3$^{fl/fl}$*) mice at indicated times after TAM injection. (F) Quantification of ZsGreen^{+} cell number in the jejunum of control *(Lgr5-CreERT2;Rosa26$^{loxp\text{-}stop\text{-}loxp\text{-}ZsGreen}$*) and *Mettl3$^{\Delta Lgr5}$* (*Mettl3$^{fl/fl}$;Lgr5-CreERT2;Rosa26$^{loxp\text{-}stop\text{-}loxp\text{-}ZsGreen}$*)mice at 1dpt (left) and 4dpt (right) hours. N=4 mice/group, n>100 crypts/group. (G) Heatmap showing the differential expression of the 384 stem cell signature genes in Lgr5-GFP^{+} ISCs from control and *Mettl3*-KO-GFP mice. (H) q-PCR shows the expression of *Mettl3*, *Lgr5*, *Ascl2*, *Olfm4*, *Lyz*, *Axin2*, *C-myc* and *Ki67* in jejunum crypts of control (*Mettl3$^{fl/fl}$*) and *Mettl3*-KO (*Vil-CreERT2;Mettl3$^{fl/fl}$*) mice after injection with Tamoxifen at indicated time. N=3 mice/group. (I) Immunofluorescence co-staining of Lgr5-GFP and KI67 in the jejunum of control and *Mettl3*-KO-GFP mice at the indicated time after TAM injection. (J) A jejunum section showing BrdU^{+} cells at 2 hours after one dose injection of BrdU in control (*Mettl3$^{fl/fl}$*) and *Mettl3*-KO (*Vil-CreERT2;Mettl3$^{fl/fl}$*) mice at 6 dpt. Quantification of BrdU-labeled cell number and crypt length at 2 hours after BrdU injection. N=3 mice/group, n>100 crypts/group. (K) Cell cycle stage distribution of the crypt epithelial cells (left) and Lgr5-GFP^{+} cells (right) in control and *Mettl3*-KO-GFP

mice at 5 dpt. N=4 mice/group. (L) Representative images (left) and quantification (right) of TUNEL$^+$ cell position in jejunum crypts of control (*Mettl3*$^{fl/fl}$) and *Mettl3*-KO (*Vil-CreERT2;Mettl3*$^{fl/fl}$) mice at the indicated time after TAM injection. The cell boundary was defined by E-cadherin. N=4 mice/group. The littermate mice (*Villin-CreERT2;Lgr5-EGFP-IRES-CreERT2;Mettl3*$^{fl/fl}$) were treated with TAM (*Mettl3*-KO-GFP) or Oil (control) (A, C, G, I, K). All the data represent mean±SD. *** P<0.001, ** P<0.01, * P<0.05, one-way ANOVA (C), two-way ANOVA (D, H, K and L), unpaired two-tailed t-test (F and J). Scale bars: 50μm (C, I, J and L), 100μm (E). Nuclei were counter-stained with DAPI.

Fig S4

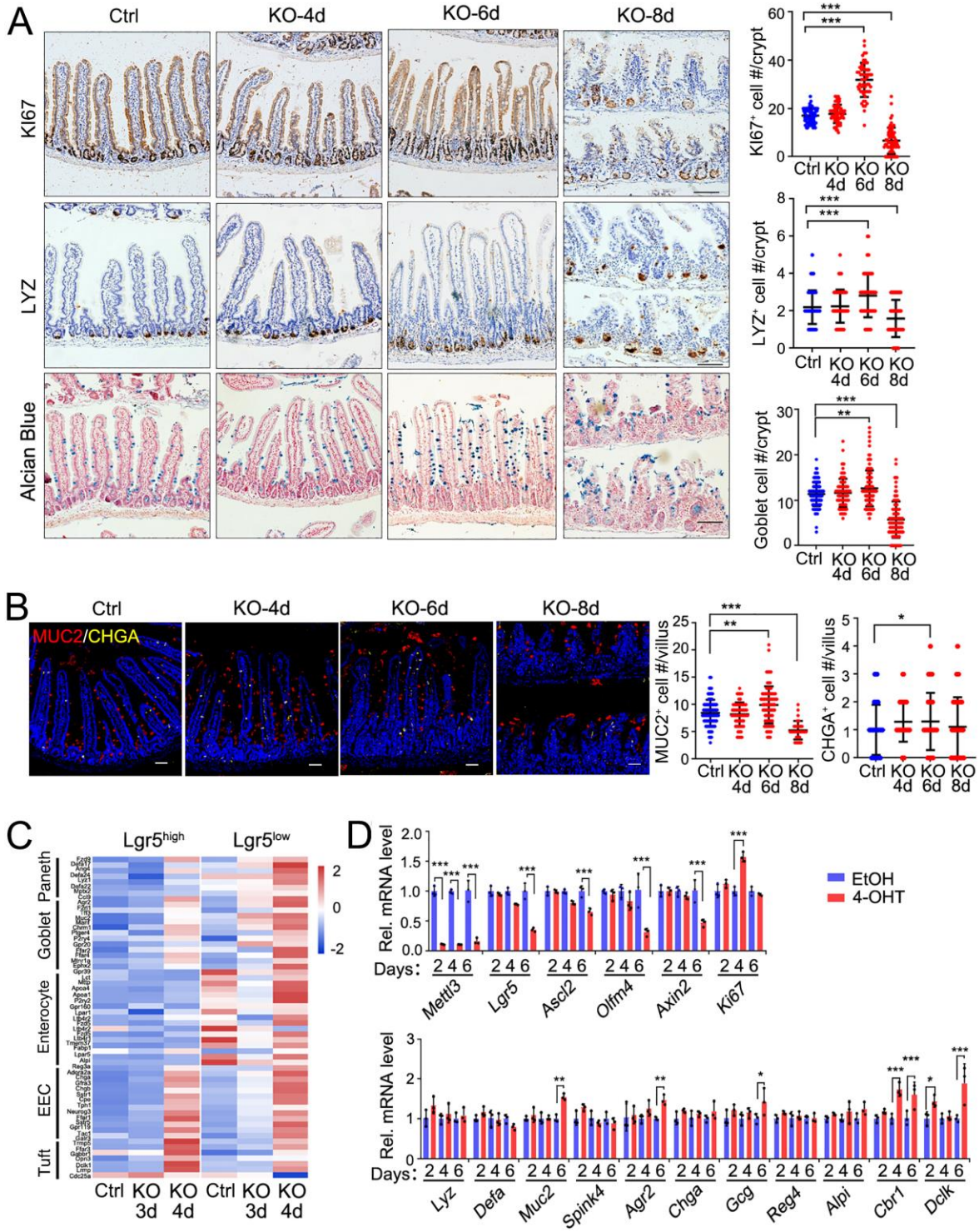

Figure S4. Mild effect on cell differentiation in *Mettl3*-KO mice, related to Figure 1.

(A) Immunohistochemical staining and quantification of KI67$^+$ cells, LYZ$^+$ cells and goblet cell (Alcian blue staining) in the jejunum of control (*Mettl3*$^{fl/fl}$) and *Mettl3*-KO (*Villin-CreERT2;Mettl3*$^{fl/fl}$) mice after injection with TAM at the indicated time. N=3 mice/group, n=5 fields/mouse, n>100 crypts or villi per group. (B) Immunofluorescence co-staining of MUC2 and CHGA and quantification (right) in the jejunum of control (*Mettl3*$^{fl/fl}$) and *Mettl3*-KO (*Villin-CreERT2;Mettl3*$^{fl/fl}$) mice after injection with TAM at

the indicated time. Nuclei were counter-stained with DAPI. N=3 mice/group, n=5 fields/mice, n>100 crypts or villi per group. (C) Expression heatmap of differentiated cell signature genes in Lgr5^{high} and Lgr5^{low} cells from control and *Mettl3*-KO-GFP mice at the indicated time. The littermate mice (*Villin-CreERT2;Lgr5-EGFP-IRES-CreERT2;Mettl3$^{fl/fl}$*) were treated with TAM (*Mettl3*-KO-GFP) or Oil (control). (D) qPCR shows gene expression in the organoids derived from *Villin-CreERT2;Mettl3$^{fl/fl}$* mice at indicated time after treated with EtOH or 4-OHT for 2 days. Data from three independent experiments were combined and shown. All the data represent mean ±SD. *** P<0.001, ** P<0.01, * P<0.05, one-way ANOVA (A, B), two-way ANOVA (D). Scale bars: 100 μm (A), 50 μm (B).

Fig S5

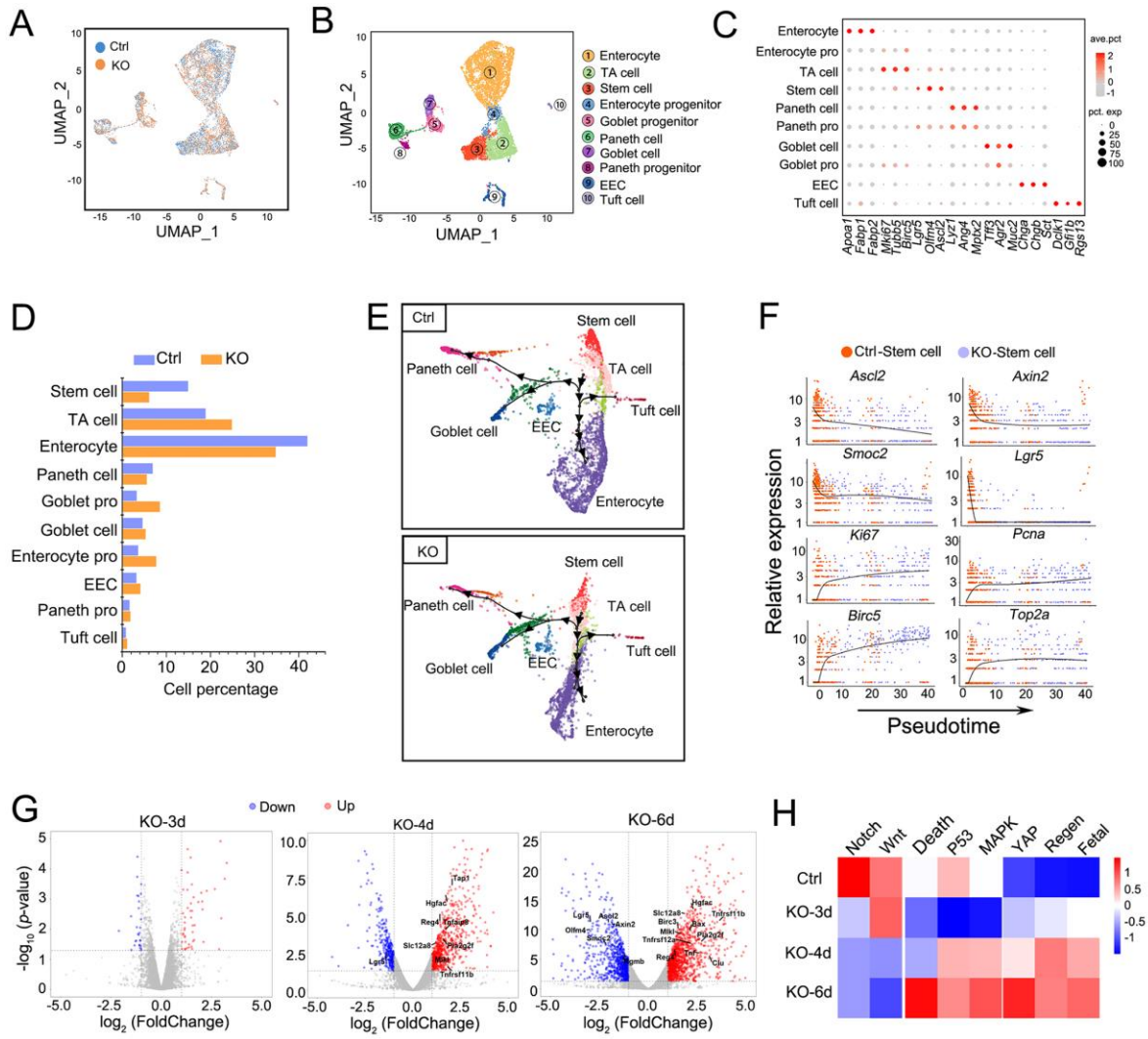

Figure S5. sc-RNA-seq analysis reveals impaired intestinal stem cells and the high proliferation property in stem cells in *Mettl3*-KO-GFP mice, related to Figure 3 and 4.

(A and B) scRNA-seq analysis of small intestinal epithelium from control and *Mettl3*-KO-GFP mice as visualized by UMAP. (C) Dot plot showing scaled expression level (color scale) and percent of expressing cells (point diameter) of the marker genes in each cell cluster. (D) The cell ratio of each cell type in the small intestinal epithelium of control and *Mettl3*-KO-GFP mice at 4 dpt. (E) Pseudotime analysis of all cell types in control and *Mettl3*-KO-GFP mice, based on scRNA-seq. The arrangement of cell clusters in *Mettl3*-KO-GFP mice on the pseudotime line was based on the cells in control mice. The points were lined according to the cell fate stage with stem cell cluster as the starting point. (F) The expression of the stem cell markers (*Ascl2*, *Axin2*, *Smoc2* and *Lgr5*) and the TA cell markers (*Ki67*, *Pcna*, *Birc5* and *Top2a*) in control stem cells and KO stem cells, plotted along the above-defined pseudotime axis in Fig. 3F. (G) Volcano plots depict differentially expressed genes in Lgr5$^+$ cells upon *Mettl3* KO for the indicated time in comparison with control mice. Red and blue dots correspond to the upregulated genes ($log_2FC \geq 1$, $p<0.05$) and downregulated genes ($log_2FC \leq -1$, $p<0.05$), respectively. (H) GSEA analysis of signaling pathways in Lgr5$^+$ ISCs upon *Mettl3* KO. NES was considered as the original values to draw the heatmap. The littermate mice (*Villin-CreERT2;Lgr5-*

EGFP-IRES-CreERT2;Mettl3$^{fl/fl}$) were treated with TAM (*Mettl3*-KO-GFP) or Oil (control).

Fig S6

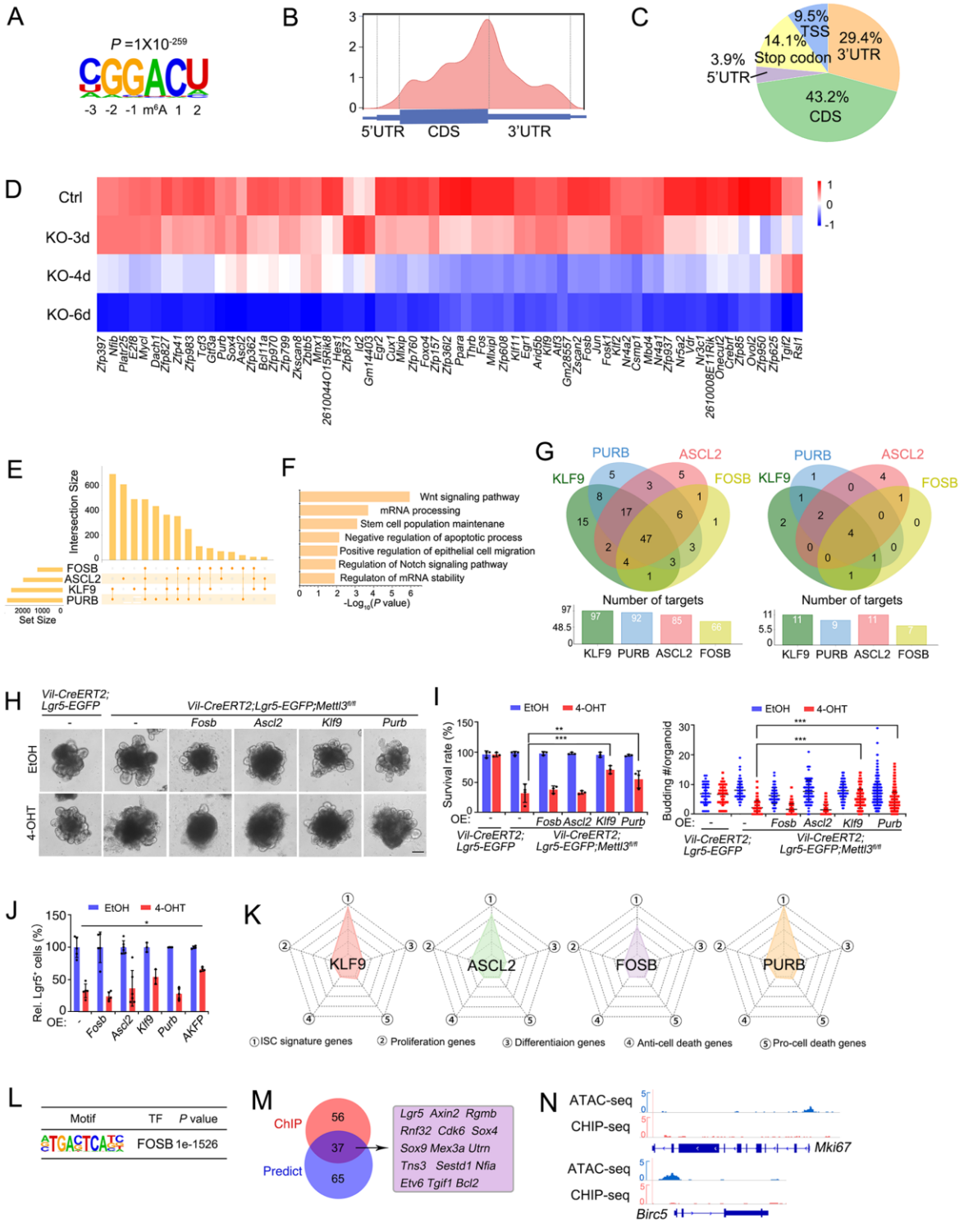

Figure S6. ASCL2, KLF9, FOSB and PURB restore the stem gene expression in the *Mettl3*-KO-GFP organoids, related to Figure 5 and 6.

(A) Consensus m6A modification sequence identified within m6A peaks by HOMER. (B and C) Metagene profiles (B) and pie chart (C) of m6A peak distribution along a normalized transcript composed of three rescaled non-overlapping segments: 5′UTR, CDS, and 3′UTR. (D) Expression

heatmap of transcription factors whose m6A modification was reduced upon *Mettl3* knockout. (E) UpsetR visualizes the overlap of the predicted target genes of AKFP. (F) GO analysis of all predicted target genes of AKFP. (G) Venn diagram indicates predicted target gene number regulated by AKFP of the down-regulated genes from 384 stem cell signature gene (left) and the 23 filter stemness gene (right). (H and I) Representative image (H), quantification of survival rate (I, left) and budding number (I, right) of the organoids expressing *Fosb*, *Ascl2*, *Klf9* or *Purb*. The organoids were derived from *Villin-CreERT2;Lgr5-EGFP-IRES-CreERT2;Mettl3*$^{fl/fl}$ or *Villin-CreERT2;Lgr5-EGFP-IRES-CreERT2* mice at day 5 after EtOH or 4-OHT treatment for 2 days. Scale bars: 100 μm. N>100 organoids/group from three independent experiments. (J) Relative Lgr5-GFP^{+} cell number in of the organoids expressing *Fosb*, *Ascl2*, *Klf9*, *Purb* or all of them (*AKFP*). The organoids were derived from *Mettl3*$^{fl/fl}$*;Villin-CreERT2;Lgr5-EGFP-IRES-CreERT2* or *Villin-CreERT2;Lgr5-EGFP-IRES-CreERT2* mice at day 6 after EtOH or 4-OHT treatment for 2 days. Data from three independent experiments were combined and shown. (K) Function characteristics distribution of the predicted target genes of KLF9, ASCL2, FOSB and PURB, respectively. (L) HOMER motif of FOSB ChIP-seq. (M) Venn diagram displays the overlap genes between predicated stem cell signature targets of Fosb (blue) and the genes confirmed by anti-FOSB ChIP-seq (red). (N) FOSB ChIP-seq and ATAC-seq tracks of the proliferation genes *Ki67* and *Birc5*. The littermate mice (*Villin-CreERT2;Lgr5-EGFP-IRES-CreERT2;Mettl3*$^{fl/fl}$) were treated with TAM (*Mettl3*-KO-GFP) or Oil (control) (A-D). All data represent mean±SD. *** P<0.001, ** P<0.01, two-way ANOVA (I and J).

Movie S1: **Time-lapse Video shows representative buds of organoids expressing Lgr5-EGFP (green) following 4-OHT treatment.** Organoids derived from *Villin-CreERT2;Lgr5-EGFP-IRES-CreERT2;Mettl3*$^{fl/fl}$ mice were imaged every 1h from day 4.5 to day 6.5 after treated with EtOH (left) or 4-OHT and labeled with CellMask (Orange plasma membrane stain, red). Video shows the change of Lgr5-GFP cells over time from 0 h to 20 h.

Table S1: Mouse model.

Label	Genotyping	Treatment
Control	*Mettl3*$^{fl/fl}$	TAM
Mettl3-KO	*Villin-CreERT2;Mettl3*$^{fl/fl}$	TAM
Control	*Lgr5-EGFP-IRES-CreERT2;Villin-CreERT2;Mettl3*$^{fl/fl}$	Oil
Mettl3-KO-GFP	*Lgr5-EGFP-IRES-CreERT2;Villin-CreERT2;Mettl3*$^{fl/fl}$	TAM
Control	*Lgr5-EGFP-IRES-CreERT2*	TAM
Mettl3-Lgr5-KO	*Lgr5-EGFP-IRES-CreERT2; Mettl3*$^{fl/fl}$	TAM
Control	*Lgr5-CreERT2;Rosa26*$^{loxp\text{-}stop\text{-}loxp\text{-}ZsGreen}$	TAM
Mettl3$^{\Delta Lgr5}$	*Lgr5-CreERT2;Rosa26*$^{loxp\text{-}stop\text{-}loxp\text{-}ZsGreen}$*;Mettl3*$^{fl/fl}$	TAM

Table S2: q-PCR primer sequences, related to Figure 2, 5, 6, S1, S3 and S4.

Gene	Forward primer	Reverse primer
Gapdh	AAGAAGGTGGTGAAGCAG	TCATACCAGGAAATGAGC
Mettl3	GGTTCGTTCCACCAGTCATAA	ATCCCATCCAGTTGGTTTCC
Lgr5	CGGGACCTTGAAGATTTCCT	GATTCGGATCAGCCAGCTAC
Ascl2	GCCTGACCAAATGCCAAGTG	ATTTCCAAGTCCTGATGCTGC
Klf9	TTATTGCACGCTGGTCACTATC	CTCATCGGGACTCTCCAGAC
Fosb	CAATCACAACCAGCCAGGAT	GGCATGTCATAAGGGTCAACA
Purb	CTTCAGCAAAGAGCCCAAATAC	CCTGCCAAGTCTTGATCCTAA
Tcf3	TTGACCCTAGCCGGACATA	CACTGGTGTCTCTCCCAAAG
Vdr	ACGCCAAGATGATCCAGAAG	GGAGATCTCATTGCCGAACA
Jun	CCTTCTACGACGATGCCCTC	GGTTCAAGGTCATGCTCTGTTT
Nr3c1	AAGCTTCGGGATGCCATTAT	TCGAGCTTCCAGGTTCATTC
Egr1	AGGAGTGATGAACGCAAGAG	GGATGGGTAAGAAGAGAGTGAAG
Fos	CGGGTTTCAACGCCGACTA	TTGGCACTAGAGACGGACAGA
Olfm4	CGAGACTATCGGATTCGCTATG	TTGTAGGCAGCCAGAGGGAG
Alpi	GTCCCACCGCTGGTTACTTT	CTGTGGGCTGAGATGATGTC
Lyz	ACGAGCTACAAACTACAACCG	GATCTCTCACCACCCTCTTTG
Axin2	GCTCCAGAAGATCACAAAGAGC	AGCTTTGAGCCTTCAGCATC
C-myc	GCTGTTTGAAGGCTGGATTTC	GATGAAATAGGGCTGTACGGAG
Ki67	AGGCTCCGTACTTTCCAATTC	CGTCTTAAGGTAGGACTTGCAG
Muc2	TGTGGTCTGTGTGGGAACTTTG	GCTTACATCTGGGCAAGTGGAA
Defa	GCACAGAAGGCTCTGCTCTT	ACCCAGATTCCACATTCAGC
Spink4	TGCAGTCACATAGCTCACAAG	CCATGCCAAGGAGGGGAA
Agr2	TGTCCCCAGAATTGTGTTTGTAGA	TGTCAGAAGGTTCATAAGCGTAGA
Chga	GCTGGAACATAAGCAGGAGG	ATCCTGCTCCATCGCTTG
Gcg	CTTCCCAGAAGAAGTCGCCA	GTGACTGGCACGAGATGTTG
Reg4	CTGAGCTGGAGTGTCAGTCAT	GTCCACTGCCATAATTGCTTCT
Cbr1	TCAATGACGACACCCCCTTC	CCTCTGTGATGGTCTCGCTTC
Dclk	CAGCAAGTCTCCCAGAAGATAC	GGACTGTGTAACAGGAGTGAAA

Table S3: sgRNA sequence, related to Figure 4.

Species	**Gene**	**Target +PAM**
Mouse	***Ascl2***	GTGGACGTTTGCACCTTCACGGG
	Klf9	CTTAAAAAGTTCTCGCGCTGGG
	Fosb	GAACCAGCTACTCAACCCCAGG
	Purb	ATCTTGAGGAAGCGGCCCTTGG
Human	***METTL3***	CTTGAGTGGCAGGAGCATCTGG
	NC	GCGCGATAGCGCGAATATAC

Table S4: RRACH enriched 3'UTR sequence, related to Figure 4.

TF		Sequence (RRACH motifs were marked with red color, A/T was marked by underline)
Ascl2	3'UTR-WT	CTTCCGGACCTTGCAGCATCAGGACTTGGAAATTTCTCAGGATAAAGATTTTTACAATGACAATCTACTTTTTATCAATTAACTTGAACTGTTGTAGGACTCTACTG
	3'UTR-mut	CTTCCGGTCCTTGCAGCATCAGGTCTTGGAAATTTCTCAGGATAAAGATTTTTACAATGACAATCTACTTTTTATCAATTAACTTGATCTGTTGTAGGTCTCTACTG
Klf9	3'UTR-WT	ATCTAAAGACTTGAAAACAAAACAACAACAACAAAAAGTTACTTATAGTCAATGGATAAGCAGAGTCCGAATTTACACTAATCAAGACAGACCTTCGAGGGGTCACGATAAGTCCGGAACTTTCAAACCTTGCTTCGTATGAATTGTACTATCTGAACATAAACTGCACT
	3'UTR-mut	ATCTAAAGTCTTGAAAACAAAACAACAACAACAAAAAGTTACTTATAGTCAATGGATAAGCAGAGTCCGAATTTACACTAATCAAGACAGACCTTCGAGGGGTCACGATAAGTCCGGATCTTTCAATCCTTGCTTCGTATGAATTGTACTATCTGATCATAATCTGCACT
Fosb	3'UTR-WT	CCGCTGAACTCGCCCTCCCTTCTTGCTCTGTAAACTCTTTAGACAAACAAAACAAACAAACCCGCAAGGAACAAGGAGGAGGAAGATGAGGAGGAGAGGGGAGGAAGCAGTCCGGGGGTGTGTGTGTGGACCCTTTGA
	3'UTR-mut	CCGCTGATCTCGCCCTCCCTTCTTGCTCTGTAAACTCTTTAGACAAACAAAACAAACAAACCCGCAAGGATCAAGGAGGAGGAAGATGAGGAGGAGAGGGGAGGAAGCAGTCCGGGGGTGTGTGTGTGGTCCCTTTGA
Purb	3'UTR-WT	CCGTATGAACCAGAGAATTATGGCTAATTCGGCTGTTACAGCCACTGGCTGGCTGCATTTTAAACCTTAAAACTTGACTATCTGCAAAAAAGGAACAGTGTGGCTACAAGCCTGAGCTTTAATGAAATAGACATCCTCACAGAGAAGTTGGAAATAACAGAACTGAAGTC
	3'UTR-mut	CCGTATGATCCAGAGAATTATGGCTAATTCGGCTGTTACAGCCACTGGCTGGCTGCATTTTAAACCTTAAATCTTGACTATCTGCAAAAAAGGATCAGTGTGGCTACAAGCCTGAGCTTTAATGAAATAGTCATCCTCACAGAGAAGTTGGAAATAACAGATCTGAAGTC

Supplemental Experimental Procedures

Immunoblotting

The following antibodies were used for immunoblotting: METTL3 (1:1000, Abcam, ab195352), ASCL2 (1:500, Abclonal, A20194), KLF9 (1:1000, Novus Biologicals, NBP-04457-100µl), FOSB (Abcam, 1:1000, ab184938), PURB (1:1000, Proteintech, 18128-1-AP), TUBULIN (1:1000,MBL, PM054-7) and GAPDH (1:1000, MBL, M171-7).

ChIP-seq

After crosslink with 1% formaldehyde and stopped with glycine, organoids were re-suspended in SDS cell lysis buffer (0.3% SDS, 50mM Tris-HCl, pH 8.0, 20mM EDTA, 1X EDTA-free protease inhibitor cocktail). The crosslinked DNA was sheared to lengths between 100 bp and 2500 bp with sonication, and diluted in DB buffer (16.7mM Tris-HCl, pH 8.0, 0.01% SDS, 1.2mM EDTA, 1.1% Triton X-100, 1X EDTA-free protease inhibitor cocktail). After pre-cleared with 30 µL of 1:1 protein A/G Dyna beads (Life Technologies, 10001D/10003D), the samples were incubated with anti-FOSB antibody (Abcam, ab184938) overnight at 4 ^{o}C, then washed 5 times with 1 mL of RIPA buffer (50mM Hepes, pH 8.0, 1% NP-40, 0.7% DOC, 0.5M LiCl, 1X EDTA-free protease inhibitor cocktail) and once with 1mL TE buffer. The beads were eluted in 100 µL of Elution buffer (10 mM Tris-HCl, pH 8.0, 1% SDS, 1 mM EDTA) for 30 min at 65 ^{o}C. The Protein-DNA complexes were reversed crosslink at 65 ^{o}C overnight. After incubation at 55 ^{o}C for 1 hour to digest proteins with 0.4mg/mL Proteinase K (AMRESCO, 0706-100mg) and another 1 hour at 37 ^{o}C to digest RNA with 0.4mg/mL RNase A (Thermo Scientific, EN0531), DNA were purified by phenol chloroform and ethanol-precipitated. Purified DNA was subjected to Tru-seq library construction using NEBNext Ultra II DNA Library Prep Kit for Illumina (NEB, E7645S). The library was purified and size-selected with AMPure XP beads (Beckman, A63881) and sequenced as paired-end with Illumina Novaseq 6000. HISAT2 was used to align the sequences to the mouse genome and generate bam files. After deprived of PCR duplicates using Picard tools, Deeptools bamCoverage (CPM normalized and extended reads) was used to generate bigwig files from bam files. MACS2 was used for peak calling and to generate bed files from aligned reads. HOMER annotatePeaks.pl was used to annotate the peaks.

MeRIP-seq analysis

The cDNA libraries were generated using SMARTER Stranded Total RNA-seq kit v2 (Takara, 634411) and sequenced on an Illumina Novaseq 6000 platform. In each sample, reads were aligned to the mouse genome in Ensembl (release 95) with HISAT2. The resulting SAM files were sorted and converted to BAM files by SAMtools and deprived of PCR duplicates using Picard tools (v1.12). m6A peaks in each sample were identified using exomePeak (v2.17.0) R/Bioconductor package with default parameters, and the corresponding input sample served as control. The significantly differential m6A peaks between Mettl3-KO-GFP and control ISCs were identified by the threshold of $|log2FC| \geq 1$ and $P<0.05$. Metagene plot was created by the Bioconductor Guitar (v2.0.0) package using the control data.

scRNA-seq normalization and clustering

Data normalization was performed using Seurat “NormalizeData” and using “LogNormalize” as the normalization method (sacle.factor=100000). Variable genes were detected using “FindVariableFeatures”. We used “FindIntegrationAnchors” to combine the control library and *Mettl3*-KO-GFP library, and the scaled gene expression data were projected onto principal components (PCs). The first 30 PCs were used for non-linear dimensionality reduction using Uniform Manifold Approximation and Projection (UMAP). Clustering was performed using the “FindNeighbors” followed

by the “FindClusters” functions. Marker genes for each cluster have been identified using “FindAllMarkers” function.

Ratio of each cell type was calculated by dividing the number of a cell type to the total number of cells. Cell cycle annotation of each cell was performed using the cell cycle scoring function in Seurat, which assigns each cell a score based on the expression of 43 marker genes for the G2/M phase and 54 marker genes for the S phase.

Gene set enrichment analysis (GSEA) and Gene ontology (GO) analysis

To define ISC signature genes, proliferation and other cellular events, we curated and referred to previous studies. Specifically, we used 384 genes that were highly expressed in $Lgr5^{high}$ ISCs (Munoz et al., 2012) for stem cell signature genes, 43 marker genes for G2/M phase and 54 marker genes for S phase for proliferation genes (Tirosh et al., 2016), Notch (HALLMARKS), Wnt (Fevr et al., 2007), P53 (HALLMARKS), MAPK (Basak et al., 2017), YAP (Imajo et al., 2015), Regeneration (Wang et al., 2019), Fetal genes (Mustata et al., 2013), differentiation genes (Haber et al., 2017) and apoptosis death-related genes (HALLMARKS).

GSEA (v.4.0) (Subramanian et al., 2005) was performed on the pre-ranked gene list as described above. Differentially expressed genes were identified using DESeq2 (v1.24.0) (Love et al., 2014). Genes with $P<0.05$ and absolute value of $|\log_2FC|>1$ were used for GO analysis, which was performed using the web tool: DAVID (Dennis et al., 2003) (http://david.abcc. ncifcrf.gov/). GO terms with $P < 0.05$ were determined to be statistically significant. Radar charts were plotted using the R software package fmsb (v0.7.1).

Motif identification

HOMER (v4.10.0) (Heinz et al., 2010) was used to call the motifs enriched in m^6A peaks or transcription factor motifs. For ChIP-seq, findMotifsGenome.pl was used to call transcription factor motifs enriched at peaks. For MeRIP-seq, findMotifs.pl was used, and the motif length was restricted to 6 nucleotides. All peaks mapped to mRNAs were used as the target sequences, and background sequences were constructed by randomly shuffling peaks upon total mRNAs using BEDTools’ shuffleBed (v2.18) (Quinlan and Hall, 2010).

scRNA-seq pseudotime analysis

Pseudotime analysis with the filtered data from Seurat was performed using Dyno (Saelens et al., 2019) and Monocle 2 (Qiu et al., 2017). Dimensionality reduction and trajectory reconstruction were carried out with the advanced nonlinear reconstruction algorithm paga_tree and DDRTree to determine two components, respectively.

Supplemental references

Basak, O., Beumer, J., Wiebrands, K., Seno, H., van Oudenaarden, A., and Clevers, H. (2017). Induced Quiescence of Lgr5+ Stem Cells in Intestinal Organoids Enables Differentiation of Hormone-Producing Enteroendocrine Cells. Cell Stem Cell *20*, 177-190 e174. 10.1016/j.stem.2016.11.001.

Dennis, G., Jr., Sherman, B.T., Hosack, D.A., Yang, J., Gao, W., Lane, H.C., and Lempicki, R.A. (2003). DAVID: Database for Annotation, Visualization, and Integrated Discovery. Genome Biol *4*, P3.

Fevr, T., Robine, S., Louvard, D., and Huelsken, J. (2007). Wnt/beta-catenin is essential for intestinal homeostasis and maintenance of intestinal stem cells. Mol Cell Biol *27*, 7551-7559.

10.1128/MCB.01034-07.

Haber, A.L., Biton, M., Rogel, N., Herbst, R.H., Shekhar, K., Smillie, C., Burgin, G., Delorey, T.M., Howitt, M.R., Katz, Y., et al. (2017). A single-cell survey of the small intestinal epithelium. Nature *551*, 333-339. 10.1038/nature24489.

Heinz, S., Benner, C., Spann, N., Bertolino, E., Lin, Y.C., Laslo, P., Cheng, J.X., Murre, C., Singh, H., and Glass, C.K. (2010). Simple combinations of lineage-determining transcription factors prime cis-regulatory elements required for macrophage and B cell identities. Mol Cell *38*, 576-589. 10.1016/j.molcel.2010.05.004.

Imajo, M., Ebisuya, M., and Nishida, E. (2015). Dual role of YAP and TAZ in renewal of the intestinal epithelium. Nat Cell Biol *17*, 7-19. 10.1038/ncb3084.

Love, M.I., Huber, W., and Anders, S. (2014). Moderated estimation of fold change and dispersion for RNA-seq data with DESeq2. Genome Biol *15*, 550. 10.1186/s13059-014-0550-8.

Munoz, J., Stange, D.E., Schepers, A.G., van de Wetering, M., Koo, B.K., Itzkovitz, S., Volckmann, R., Kung, K.S., Koster, J., Radulescu, S., et al. (2012). The Lgr5 intestinal stem cell signature: robust expression of proposed quiescent '+4' cell markers. EMBO J *31*, 3079-3091. 10.1038/emboj.2012.166.

Mustata, R.C., Vasile, G., Fernandez-Vallone, V., Strollo, S., Lefort, A., Libert, F., Monteyne, D., Perez-Morga, D., Vassart, G., and Garcia, M.I. (2013). Identification of Lgr5-independent spheroid-generating progenitors of the mouse fetal intestinal epithelium. Cell Rep *5*, 421-432. 10.1016/j.celrep.2013.09.005.

Qiu, X., Mao, Q., Tang, Y., Wang, L., Chawla, R., Pliner, H.A., and Trapnell, C. (2017). Reversed graph embedding resolves complex single-cell trajectories. Nat Methods *14*, 979-982. 10.1038/nmeth.4402.

Quinlan, A.R., and Hall, I.M. (2010). BEDTools: a flexible suite of utilities for comparing genomic features. Bioinformatics *26*, 841-842. 10.1093/bioinformatics/btq033.

Saelens, W., Cannoodt, R., Todorov, H., and Saeys, Y. (2019). A comparison of single-cell trajectory inference methods. Nat Biotechnol *37*, 547-554. 10.1038/s41587-019-0071-9.

Subramanian, A., Tamayo, P., Mootha, V.K., Mukherjee, S., Ebert, B.L., Gillette, M.A., Paulovich, A., Pomeroy, S.L., Golub, T.R., Lander, E.S., et al. (2005). Gene set enrichment analysis: a knowledge-based approach for interpreting genome-wide expression profiles. Proc Natl Acad Sci U S A *102*, 15545-15550. 10.1073/pnas.0506580102.

Tirosh, I., Izar, B., Prakadan, S.M., Wadsworth, M.H., 2nd, Treacy, D., Trombetta, J.J., Rotem, A., Rodman, C., Lian, C., Murphy, G., et al. (2016). Dissecting the multicellular ecosystem of metastatic melanoma by single-cell RNA-seq. Science *352*, 189-196. 10.1126/science.aad0501.

Wang, Y., Chiang, I.L., Ohara, T.E., Fujii, S., Cheng, J., Muegge, B.D., Ver Heul, A., Han, N.D., Lu, Q., Xiong, S., et al. (2019). Long-Term Culture Captures Injury-Repair Cycles of Colonic Stem Cells. Cell *179*, 1144-1159 e1115. 10.1016/j.cell.2019.10.015.